iScience

CellPress
OPEN ACCESS

Article

Single-cell sequencing of immune cells from the coronary sinus reveals immune mechanisms of the progression of persistent atrial fibrillation

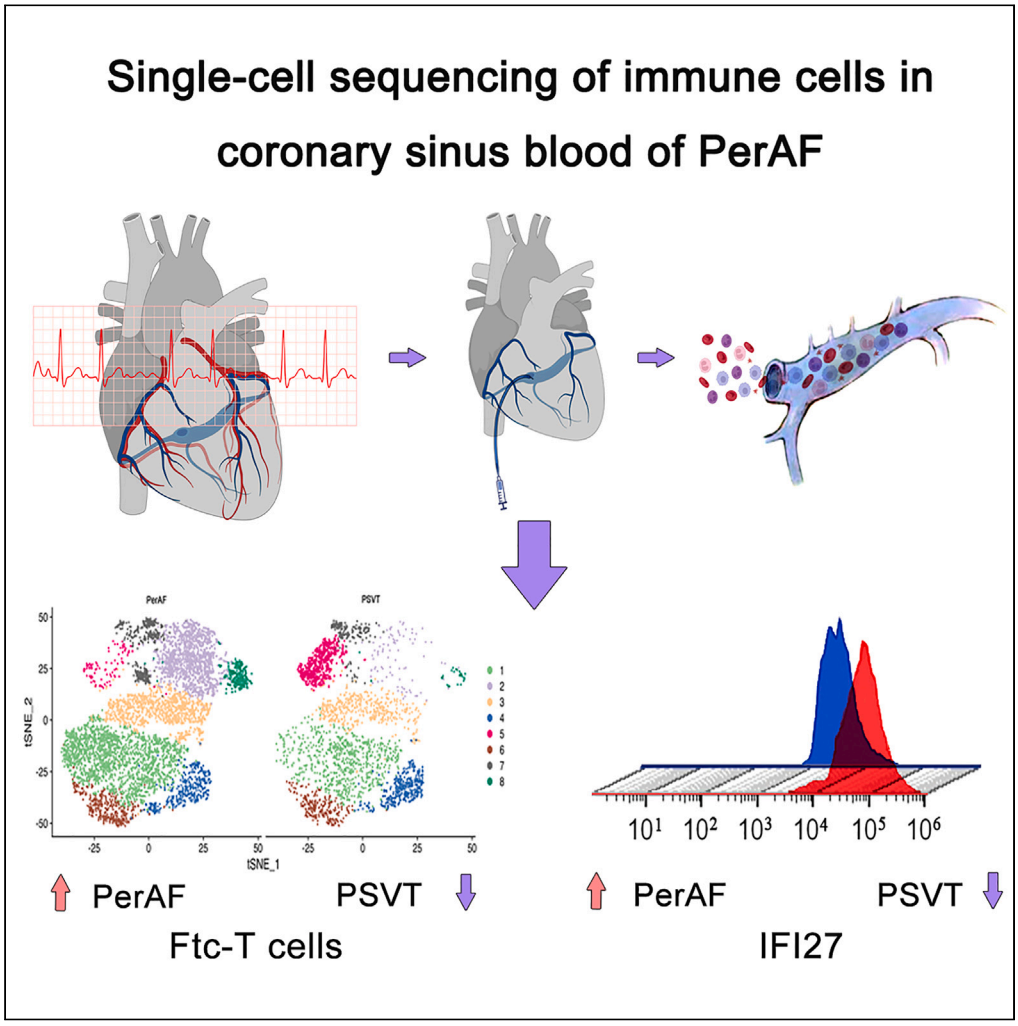

Chaofeng Chen, Yang Pang, Kuan Cheng, ..., Qingxing Chen, Wen-qing Zhu, Jun-bo Ge

chenqxsci@163.com (Q.C.)
20111210013@fudan.edu.cn (W.-q.Z.)

Highlights

T cell remodeling in coronary sinus blood of persistent atrial fibrillation (PerAF)

FGFBP2(+)TRDC(−) CD4(−) T (Ftc-T) cells were enriched in coronary sinus blood of PerAF

Ftc-T cells was closely associated with AF recurrence post catheter ablation

IFI27 is highly expressed in PerAF and is closely related to myocardial fibrosis

Chen et al., iScience 27, 110127
June 21, 2024
https://doi.org/10.1016/j.isci.2024.110127

iScience

CellPress
OPEN ACCESS

Article

Single-cell sequencing of immune cells from the coronary sinus reveals immune mechanisms of the progression of persistent atrial fibrillation

Chaofeng Chen,[1,2,4] Yang Pang,[1,4] Kuan Cheng,[1,4] Xiaofei Gao,[2] Yunlong Ling,[1] Ye Xu,[1] Jing Wu,[2] Yi-zhou Xu,[2] Qingxing Chen,[1,3,*] Wen-qing Zhu,[1,5,*] and Jun-bo Ge[1]

SUMMARY

Identifying the atlas of immune cells from coronary sinus circulation (CSC) of patients with persistent atrial fibrillation (PerAF) may provide new insights into the role of immune cells in the progression of AF. Single-cell sequencing revealed substantial alterations in immune cells from CSCs of patients with PerAF, especially a markedly elevated abundance of T cells, after which we identified a T cell subset: FGFBP2(+)TRDC(−)CD4(−) T cells (Ftc-T cells), which can promote the proliferation of cardiac fibroblasts (CFs),and the proportion of Ftc-T had a positive linear with AF recurrence post catheter ablation (CA). Moreover, IFI27 was found to be highly enriched in Ftc-T cells and promoted CFs proliferation and collagen expression. Altogether, our findings represent a unique resource providing in-depth insights into the heterogeneity of the immune cell from CSC of patients with PerAF and highlight the potential role of Ftc-T cells and IFI27 for AF progression.

INTRODUCTION

Atrial fibrillation (AF) is a prevalent cardiac arrhythmia that significantly impacts individuals worldwide, often resulting in reduced long-term survival and heightened healthcare costs.[1] Although catheter ablation (CA) is an effective treatment for AF, it is accompanied by a high recurrence rate for persistent AF (PerAF) over the long term.[2] The progression of AF and its recurrence post-CA may closely correlate with the persistent progression of atrial fibrosis.[3] Although the precise biological mechanisms disrupting atrial electrical stability and causing persistent progression of atrial fibrosis remain incompletely understood, inflammation and immune response may contribute to this progression.[4]

The role of inflammatory and immune response in the development of atherosclerosis and heart failure (HF) has been well established.[5] Increasing evidence also supports the role of immune response in the pathology of AF.[6] Patients with AF were found to have elevated levels of inflammatory markers and neutrophil/lymphocyte ratio (NLR) compared with the general population.[4,7] Inflammation can alter atrial electrophysiology and structural substrates, thereby leading to the onset and persistence of AF.[8] In turn, AF might lead to calcium overload in atrial myocytes, resulting in cell death, danger-associated molecular pattern (DAMP) release, and subsequent inflammatory response activation.[9] Therefore, inflammation and immune response are involved in the initiation and maintenance of AF, whereas AF can promote inflammation, leading to an 'AF begets AF' phenomenon.

The inflammation and immune response associated with AF tend to be a persistent yet low-grade nature, believed to be more conducive to the progression of atrial fibrosis.[10] The enduring inflammatory state of AF is closely tied to the infiltration of immune cells and cytokines. Previous studies have demonstrated the involvement of T cells in the atherosclerosis process.[11] Furthermore, immune cell infiltration, predominantly characterized by macrophages and T cells, has been identified in the left atrial appendage (LAA) of PerAF patients, suggesting that T cell-mediated immune responses may play a role in the pathology of AF. However, multiple subtypes of T cells exist, each with distinct roles in inflammation and fibrosis, and the abundance of a particular subtype may have a more pronounced impact.[12] Because the proportion of immune cells in the blood perfusion tissue may indirectly mirror their abundance in the tissue, the prevalence and functional significance of T cell subtypes in cardiac tissue may be indirectly represented by their proportion in the cardiac circulation.

The coronary sinus (CS) serves as the gathering place for blood collection following cardiac circulation. In comparison to peripheral blood, blood derived from the CS may possess more cardiac information.[13,14] Consequently, the composition and proportion of immune cells in the cardiac circulation of AF patients could offer a more insightful reflection of the impact of immune cells on the pathological processes of AF. Despite this potential, the specific signatures of immune cells from the CS circulation (CSC) in AF patients remain unknown, and there is currently a lack of reported studies addressing this aspect.

[1]Department of Cardiology, Zhongshan Hospital, Fudan University, Shanghai Institute of Cardiovascular Diseases, Shanghai 200000, China
[2]Department of Cardiology, Hangzhou First People Hospital, 261 Huansha Road, Hangzhou 310000, China
[3]The Second People's Hospital of Kashi, Xinjiang, China
[4]These authors contributed equally
[5]Lead contact
*Correspondence: chenqxsci@163.com (Q.C.), 20111210013@fudan.edu.cn (W.-q.Z.)
https://doi.org/10.1016/j.isci.2024.110127

Table 1. Characteristics of patients undergoing single-cell RNA sequencing

Characteristics	PerAF (n = 3)				PSVT (n = 3)				p-value
Age, years	54	58	53	55 ± 2.6	49	59	55	54 ± 5	0.77
Male, n (%)	Male	Male	Male	3 (100%)	Male	Male	Male	3 (100%)	1
BMI, kg/m^2	22.6	24.8	25.3	24.2 ± 1.4	23.8	26.1	24.3	24.7 ± 1.2	0.66
Duration of AF, months	12	10	13	11.7 ± 1.5	–	–	–		–
LVEF, (%)	61.5	62.1	60.5	61.4 ± 0.8	62.4	61.4	62.2	62 ± 0.5	0.32
LAD, mm	43.2	40.5	44.1	42.6 ± 1.9	33.4	32.1	34.5	33.3 ± 1.2	0.002
Hy, n (%)	1	1	0	2 (66.3%)	1	1	1	3 (100%)	1.00
CHD, n (%)	0	0	1	1 (33.3%)	0	0	0	0	1.00
Current or former smoker (%)	1	0	0	1 (33.3%)	0	1	1	2 (66.7%)	1.00

Values are mean ± SD or n (%). PerAF, persistent atrial fibrillation, PSVT, paroxysmal supra-ventricular tachycardia, CHD, coronary heart disease, Hy, hypertension, BMI, Body mass index, LAD, left atrial diameter, LVEF, left ventricular ejection fraction. The statistical method used was Fisher exact test for comparison of categorical variables, and a Mann-Whitney U test for comparison of continuous variables. Statistical tests were 2-tailed, with $p < 0.05$ indicating statistical significance.

Paroxysmal supraventricular tachycardia (PSVT) is a common cardiac arrhythmia, typically characterized by its benign and self-limiting nature. The anatomical basis of PSVT lies in the congenital presence of one or more abnormal conduction pathways in the atrioventricular junction area. However, other physiological characteristics and biological indicators of PSVT do not significantly different those of the general population. Therefore, PSVT is commonly utilized as a control group in research related to AF.

Herein, we opted for PSVT as our control group, subsequently pioneering the creation of a single-cell RNA sequencing (scRNA-seq) atlas of immune cells in CSC of patients with PerAF. This initiative provides a more profound understanding of the signatures and heterogeneity of immune cells in the CSC of individuals with PerAF. Notably, our dataset unveiled a subset of T cells, denoted as FGFBP2(+)TRDC(−) CD4(−) T cells T cells (Ftc-T cells), showcasing a positive linear correlation with AF and AF recurrence post-ablation. Furthermore, IFI27 exhibited significant enrichment in Ftc-T cells. Therefore, Ftc-T cells may participate in the pathological process of atrial fibrosis progression in PerAF through IFI27 and the JAK/STAT signaling pathway, presenting a potential target for immunological interventions in patients with PerAF.

RESULTS

Single-cell transcriptome atlas of immune cells from the CS in patients with PerAF

We isolated coronary sinus blood mononuclear cells (CBMCs) from individuals with PerAF and compared them with PSVT controls. Subsequently, we conducted scRNA-seq using the 10xGenomics platform (patient characteristics are presented in Table 1). After rigorous quality controls (QC), involving the filtration of cells with low RNA content or high mitochondrial RNA, we identified 11,146 cells per sample, with an average of 1,819 genes per cell and 5542 mean UMI counts per cell (refer to Table S1 and Figure S1). The data were aggregated into a t-SNE plot (Figure 1A), revealing 15 clusters of cells (Figures 1B and 1C) with different proportions (Figure 1D and details in Table S2). The heatmap displayed the top 10 marker genes in each cluster (Figure 1E). Moreover, the feature and violin plot of the top marker genes of clusters are displayed in Figure S2. The t-SNE projection plot highlighted a higher proportion of clusters 3, 4, and 5 in the PerAF group, surpassing those in the PSVT group (31.21% ± 2.22% vs. 9.12% ± 1.2%, $p < 0.001$; 22.56% ± 1.22% vs. 0.86% ± 0.21%, $p < 0.001$, and 15.68% ± 1.03% vs. 4.84% ± 0.99%, $p < 0.001$, details in Table S2).

Characterization of CBMCs in patients with PerAF

Referring to the transcriptomic datasets from 'Human Primary Cell Atlas',[15] as illustrated in heatmap (Figure 2A) and t-SNE plot (Figure 2B and 2C), the bio-informatics cell annotation utilizing marker genes revealed that the majority of cells correspond to the five general immune cells types: T-lymphocyte cells (T cells 53.9%, cluster 3, 5and 7), followed by monocytes (30.9%, cluster1, 8, 12 and 15) and natural killer cells (NK cells 13.4%, cluster 2, 4 and 6), B-lymphocyte cells (B cells 5.3%, cluster 9, 10, 11 and 14), and Dendritic cells (DC 1.2%, cluster 13) (Figure 2A).Furthermore, the PerAF group exhibited a significant increase in T cells compared with the PSVT group (71.2% ± 5.45%vs. 34.4% ± 3.01%, $p < 0.001$) (Figure 2D, Table S3). In contrast, the proportion of monocyte and NK cells was relatively lower in the PerAF group (details in Table S3). High T cell abundance (as determined by flow cytometry analysis) was validated in the independent cohort (60.8% vs. 36.2%, $p < 0.001$) (Figures 2E and 2F).

In comparison to the PSVT group, the PerAF group exhibited 41 significantly up-regulated genes and 169 significantly down-regulated genes, as illustrated in the heatmap displaying the top 25 differentially expressed genes (DEGs) (Figure 2G). Figure 2H further illustrates the DEGs excluding immunoglobulin genes. The up-regulated DEGs encompassed T cell-related marker genes (*CD8A/CD8B/CD3D/CD3G/CD52/CD69/CCL5/LY6E*), *IFN*-stimulated genes (*IFI44L/IFI27/IFI6/ISG15*), membrane protein genes (*LIME1* and *LTB*), and genes involved in the regulation of RNAs and DNAs (*NCOR2/MX1*), among others. To understand the interactions among these genes, we

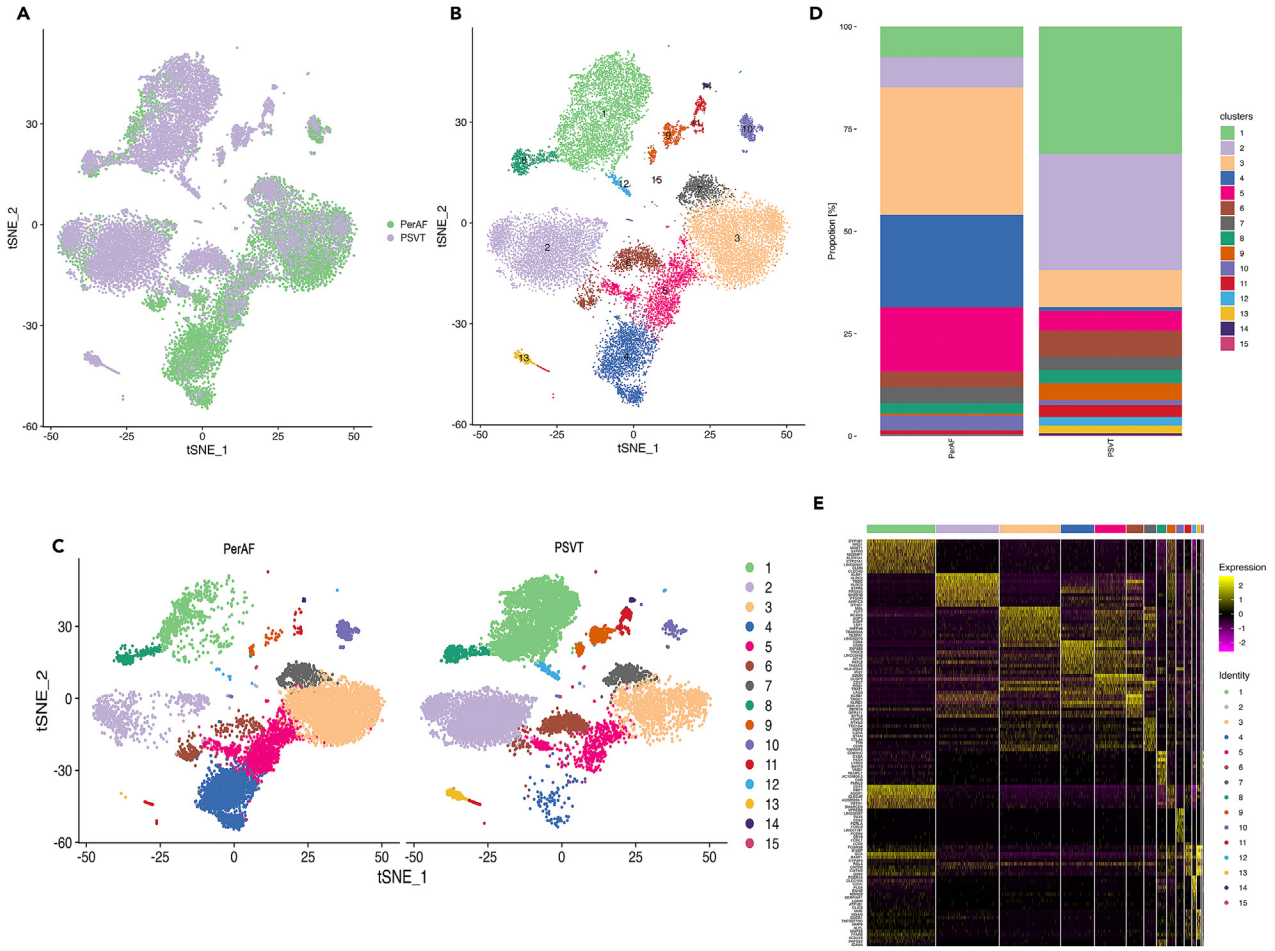

Figure 1. T-SNE projection plot of scRNA-seq data of CBMCs from PerAF and PSVT

(A) T-SNE projection output of all single cells of CBMCs from PerAF (green) and PSVT (purple) subjects, each dot corresponds to a single cell.

(B) T-SNE projection plot of CBMCs, showing the identification of 15 main clusters. Each dot corresponds to a single cell, colored according to the cell cluster.

(C) T-SNE projection plot of CBMCs yielded 15 clusters for PerAF (left) and PSVT (right) subjects respectively. Each dot corresponds to a single cell, colored according to the cell cluster.

(D) Different clusters fractions of CBMCs from PerAF (left) and PSVT (right) subjects, colored according to the cell cluster (N = 15).

(E) Heatmap of top 10 marker genes of the different clusters, colored according to the cell cluster (N = 15). ScRNA-seq, single-cell ribonucleic acid sequencing; PerAF, persistent atrial fibrillation; PSVT, paroxysmal supra-ventricular tachycardia; CBMCs, coronary sinus blood mononuclear cells; T-SNE, T-distributed stochastic neighbor embedding.

constructed a PPI network using Metascape (Figure 2I). The network revealed that most of the DEGs are associated with one another. Notably, the genes cluster: "*CD8A/CD8B/CD3D/CD3G/CD52/CD69*" was associated with *IFN*-stimulated genes, membrane protein genes, *IL32*, *NCOR2* and *MT2A* either directly or indirectly. *CD69*, a marker gene for T cell activation, and *CCL5*, a marker gene for $CD8^+$ T cells, suggest that this specific cell subtype may represent a group of activated $CD8^+$ T cells. These cells may function by regulating the secretion of cytokines, influencing the expression of membrane proteins, and interfering with the translation and transcription of genes, among other mechanisms.

As immunoglobulin genes are not part of the regular transcriptome, and their inclusion might impact the result of the GO analysis, we conducted an analysis excluding immunoglobulin genes. The DEGs without immunoglobulin genes were subjected to enrichment analysis in the KEGG and GO database. The KEGG classification enrichment highlighted a significant proportion of DEGs primarily influenced the "immune system, endocrine system, and circulatory system" in Organismal Systems, and their contribution to "infectious diseases, endocrine and metabolic diseases, and cardiovascular diseases" within Human Diseases. Additionally, they played roles in "signaling molecules and interaction, signal transduction" in Environment Information Processing, and were involved in "transport and catabolism, cell growth and death" in Cellular Processes (Figure 2J). Further KEGG pathway enrichment analysis of the DEGs revealed highly enriched pathways, including rheumatoid arthritis, T cell receptor signaling pathway, Th17 cell differentiation, Th1 and Th2 cell differentiation, NF-kappaβ signaling pathway, Ferroptosis, Phagosome, Lysosome, and others (Figure 2K). Functional enrichment analysis using the GO database showcased

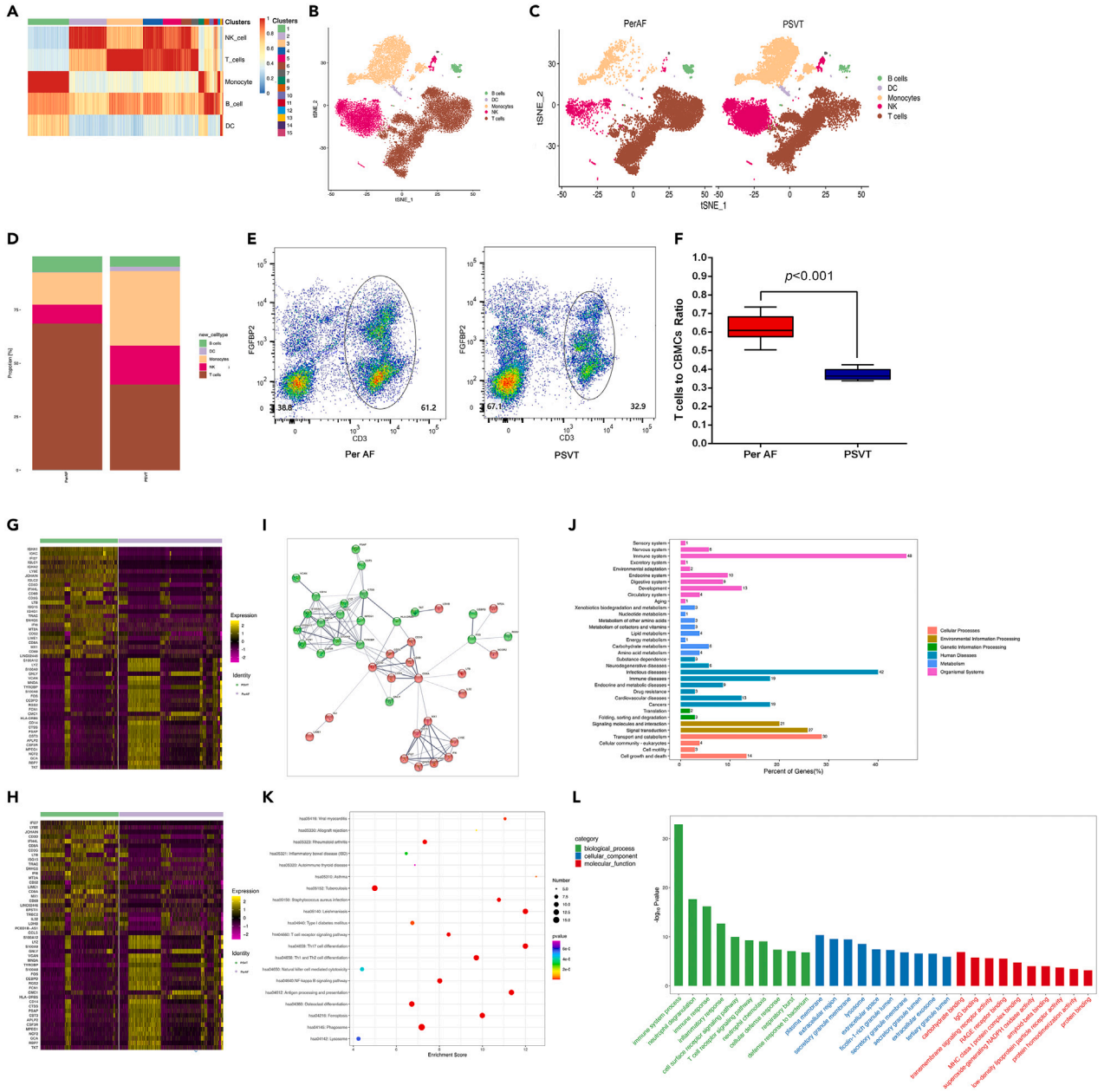

Figure 2. Identification and annotation of CBMCs between PerAF and PSVT subjects

(A) Heatmap showing of different clusters matching traditional immune cell types.

(B) T-SNE projection plot of CBMCs matched for traditional immune cell types. Each dot corresponds to a single cell, colored according to immune cell types.

(C) T-SNE projection plot of CBMCs from PerAF (left) and PSVT (right) subjects matched for traditional immune cell types, respectively. Each dot corresponds to a single cell, colored according to immune cell types.

(D) Abundance distribution of different immune cells of CBMCs of the PerAF (left) and PSVT (right) subjects.

(E and F) Validation of the differential distribution of immune cells in the CSC of PerAF (left) and PSVT (right) subjects. (E) Flow cytometry analysis of differential distribution of immune cells in the CSC of PerAF (left) and PSVT (right) subjects in the validation cohort. (F) High abundance distribution of T cell were identified in CBMCs of PerAF patients, $N = 10$ vs. 10, two-tailed unpaired Student's t tests, $p < 0.05$ indicating statistical significance.

(G) Heatmap of top DEGs of CBMCs between PerAF and PSVT subjects.

(H) Heatmap of top DEGs without immunoglobulin genes of CBMCs between PerAF and PSVT subjects.

(I) PPI network of DEGs without immunoglobulin genes of CBMCs between PerAF and PSVT subjects.

(J) KEGG classification enrichment analysis of DEGs without immunoglobulin genes of CBMCs between PerAF and PSVT subjects.

(K) KEGG pathway enrichment analysis of DEGs without immunoglobulin genes of CBMCs between PerAF and PSVT subjects.

Figure 2. *Continued*

(L) GO enrichment analysis of DEGs without immunoglobulin genes between PerAF and PSVT subjects. PerAF, persistent atrial fibrillation; PSVT, paroxysmal supra-ventricular tachycardia; T-SNE, T-distributed stochastic neighbor embedding; CSC, Coronary sinus circulation. CBMCs, coronary sinus blood mononuclear cells; DEGs, differentially expressed genes; PPI, protein–protein interaction; GO, gene ontology; KEGG, Kyoto Encyclopedia of Genes and Genomes.

major terms in the biological process (BP), such as immune system, neutrophil degranulation, cell surface receptor signaling pathway, and T cell receptor signaling pathway, among others. In terms of cellular component (CC), most of the genes were enrichment in plasma membrane, secretory granule membrane, lysosome, extracellular space, extracellular exosome, etc. Moreover, the significantly enriched molecular function (MF) term included carbohydrate binding, IgG binding, transmembrane signaling receptor activity, RAGE receptor binding, and protein binding, among others (Figure 2L).

Characterization of T cells from CBMCs in patients with PerAF

Given that T cells constituted the largest population exhibiting substantial transcriptional changes associated with AF (Figure 3A), we subsequently re-clustered the entire T cell population to investigate the influence of T cells on AF and identify differentially regulated genes. The t-SNE output revealed 11 clusters representing different T cell subtypes (Figure 3B and 3C) with varying proportions, notably cluster 2,exhibited a significantly higher proportion in T cells from PerAF patients compared to the PSVT group (28.8% $\pm$ 3.34% vs. 3.1% $\pm$ 1.12%, $p < 0.001$) (Figure 3D and details in Table S4). The heatmap displayed the top 10 marker genes of each cluster (Figure 3E), and the feature and violin plot of the top markers gene of clusters are displayed in Figure S3.

Compared with the PSVT group, we identified 37 significantly up-regulated and 16 significantly down-regulated genes were identified in T cells of the PerAF group. The top DEGs of T cells closely mirrored those observed in CBMCs between the two groups (Figure 3F). Additionally, the KEGG classification analysis suggested that these DEGs acted on the immune system, infectious and cardiovascular diseases and were associated with signaling molecules and interaction, signal transduction and transport, and cell grown and death (Figure 3G). KEGG pathway enrichment indicated that many genes were enriched in the rheumatoid arthritis, Influenza A, T cell receptor signaling pathway, Th1 and Th2 cell differentiation, NF-kappaβ signaling pathway, Ferroptosis etc.(Figure 3H). Additionally, the DEGs of T cells were associated with GO terms related to type I interferon signaling pathway, immune response, T cell receptor signaling pathway in terms of BP; extracellular region, cell surface, mitochondrion, extracellular exosome, plasma membrane, endosome in terms of CC; protein homodimerization activity, protein binding, RAN binding and DNA binding in terms of MF (Figure 3I).

Characterization of T cells subtypes from CBMCs in patients with PerAF

Match with the known marker genes of various T cells (Table S5), which mainly include CD4 naive T cells, CD4 effector T cells, CD4 Treg cells, CD8 naive T cells, CD8 cytotoxic T cells, GdT (γδT) cells, NKT cells (Figure 4A). In the t-SNE output, a significantly higher proportion of cytotoxic $CD8^+$ cells and exhausted $CD8^+$T (T-ex) cells were identified in PSVT (44.4% $\pm$ 5.51% vs. 17.0% $\pm$ 3.12%, $p < 0.001$) (Figure 4B and 4C, Table S6). The clusters of T cells were matched with the marker genes of general T cell subsets, indicating that cells in the cluster2 were mainly cytotoxic $CD8^+$ cells and exhausted $CD8^+$T (T-ex) cells (Figure 4D).

In cluster 2 of T cells, 63 genes were significantly up-regulated, and 16 genes were significantly down-regulated (Top 25 DEGs) (Figure 4E). Intriguingly, we observed that the top DEGs in cluster 2 were similar to those in CBMCs and T cells (Table S7). KEGG classification analysis indicated that these DEGs functioned in the immune and circulatory system, as well as in infectious and cardiovascular diseases. They were also associated with signaling molecules and interaction, signal transduction, and cell growth and death (Figure 4F). KEGG pathway enrichment revealed that DEGs were primarily enriched in the T cell receptor signaling pathway, Th17 cell differentiation, Th1 and Th2 cell differentiation, Jak/STAT signaling pathway, PI3K/Akt signaling pathway, and RNA transport, among others (Figure 4G). Furthermore, GO enrichment demonstrated that, in terms of biological processes (BP), most terms were associated with the immune response, type I interferon signaling pathway, and T cell receptor signaling pathway; in cellular components (CC), most terms were associated with the plasma membrane, extracellular exosome, endosome membrane, etc. Regarding molecular functions (MF), most terms were associated with antigen binding, immunoglobulin receptor binding, carbohydrate binding, RNA binding, transmembrane signaling receptor activity, GTP binding, and DNA-binding transcription factor activity, among others (Figure 4H).

Collectively, the KEGG and GO enrichment analysis of cluster 2 were akin to those observed in T cells. Hence, it is plausible that cluster 2 represents functionally significant cells among immune cells, playing a crucial role in the pathological processes of PerAF and maintaining a close association with PerAF.

The redefinition and function of cluster2

FGFBP2 was the top marker gene of cluster 2 (Figure 3E).However, beyond cluster 2, cells expressing *FGFBP2* were also scattered in cluster 7, 8 and 11 (Figures 3E and 5A-a).To refine the representation of cluster 2, we selectively excluded *FGFBP2* expressing cells from cluster 7, 11 (Figure 5A-b) and 8 (Figure 5A-d). This exclusion process aimed to enhance the precision of *FGFBP2* expressing cells, more accurately reflecting the characteristics of cluster 2. Notably, *TRDC* and *CD4* served as marker genes for cluster 7, 11 and 8 (Figure 3E). Co-expressing *TRDC* with *FGFBP2* and *CD4* with *FGFBP2* accounted for 95.6% and 96.3% of cluster 7, 11 and 8 (Figures 5A-c and 6A-e). As shown in the t-SNE output, cells expressing *FGFBP2* but not *TRDC* and *CD4* (FGFBP2(+)TRDC(−)CD4(−) T cells) (Figure 5A-f) closely aligned with cluster 2 (95.3%) (Figure 5A-g). Consequently, we apply FGFBP2(+)TRDC(−) CD4(−) T cells (Ftc-T cells) to represent Cluster 2.

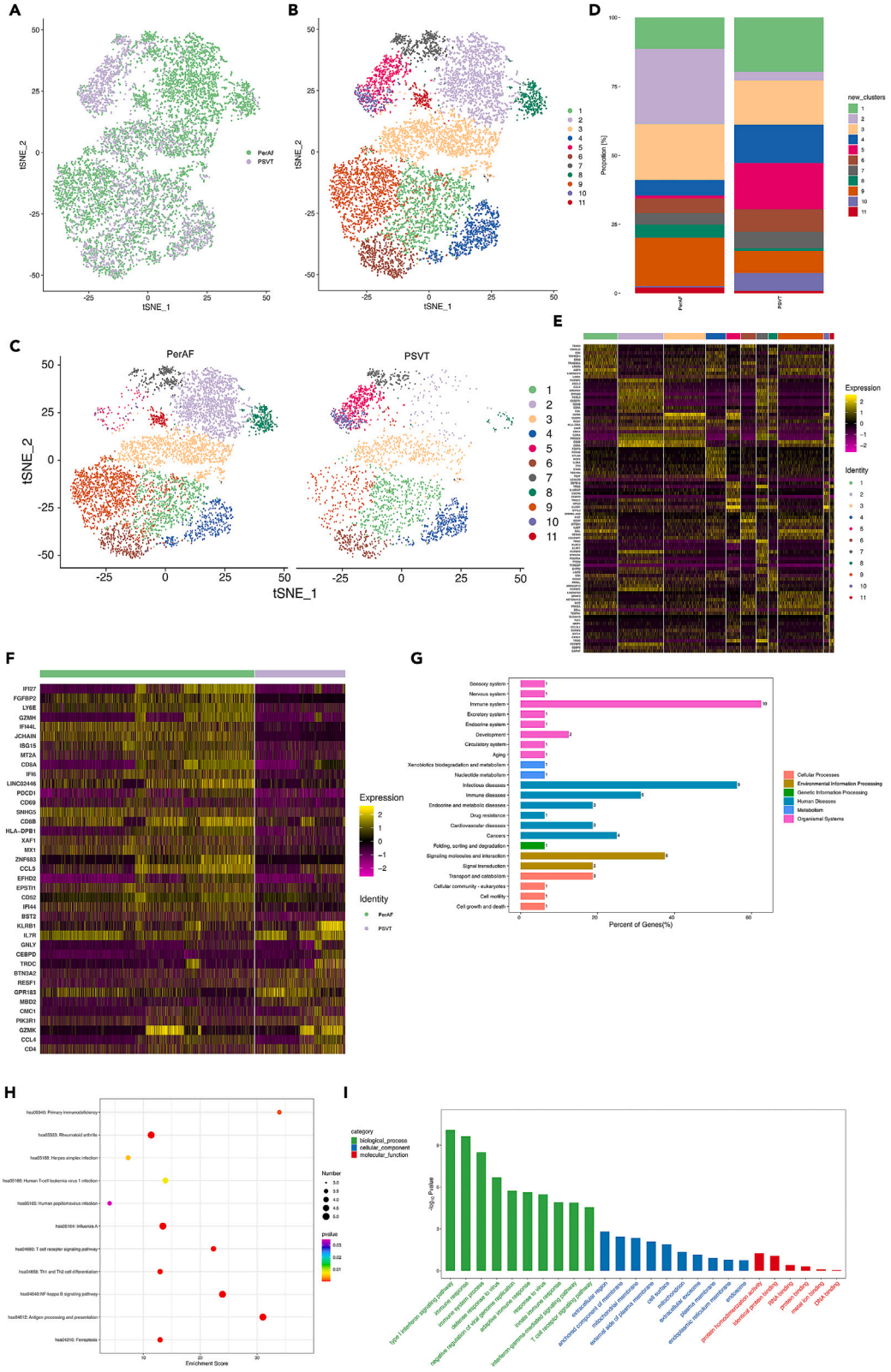
A
B
C
D
E
F
G
H
I
PerAF
PSVT
tSNE_1
tSNE_2
new_clusters
Proportion (%)
Expression
Identity
Percent of Genes(%)
Enrichment Score
category
biological_process
cellular_component
molecular_function

Figure 3. ScRNA-seq data analysis of T cells between PerAF and PSVT subjects

(A) T-SNE projection plot of T cells of CBMCs between PerAF and PSVT subjects.

(B) Dimensional reduction t-SNE projection plot of scRNA-seq data of T cells yielded 11 clusters.

(C) Dimensional reduction t-SNE projection output of scRNA-seq data of T cells for PerAF (right) and PSVT (left) subjects yielded 11 clusters, respectively.

(D) Abundance distribution of different clusters of T cells from CBMCs between the PerAF (left) and PSVT (right) subjects.

(E) Heatmap of top 10 marker genes for clusters of T cells of CBMCs between PerAF and PSVT subjects.

(F) Heatmap of top DEGs without immunoglobulin genes of T cells from CBMCs between PerAF and PSVT subjects.

(G) KEGG classification enrichment analysis of DEGs without immunoglobulin genes of T cells from CBMCs between PerAF and PSVT subjects.

(H) KEGG pathway enrichment analysis of DEGs without immunoglobulin genes of T cells from CBMCs between PerAF and PSVT subjects.

(I) GO enrichment analysis of DEGs without immunoglobulin genes of T cells from CBMCs between PerAF and PSVT subjects. scRNA-seq, single-cell ribonucleic acid sequencing; PerAF, persistent atrial fibrillation; PSVT, paroxysmal supra-ventricular tachycardia; T-SNE, T-distributed stochastic neighbor embedding; CBMCs, coronary sinus blood mononuclear cells; DEGs, differentially expressed genes; GO, gene ontology; KEGG, Kyoto Encyclopedia of Genes and Genomes.

Subsequently, we employed the Ftc-T cells to the total T cells ratio (FTR) and CBMCs ratio (FCR) to gauge the abundance of Ftc-T cells. In the validation cohort, flow cytometry analysis confirmed significantly higher FTR and FCR in the PerAF group compared to the PSVT group (Figure 5B and 5C) (FTR: 27.31 $\pm$ 3.11% vs.7.24% $\pm$ 1.38%, $p < 0.001$(Figure 5D); FCR: 17.19 $\pm$ 2.71% vs. 2.95 $\pm$ 0.87%, $p < 0.001$, (Figure 5E)). Moreover, the further cell experiments *in vitro*, we co-cultured Ftc-T cells with cardiac fibroblasts (CFs) and observed a substantial promotion of CF proliferation by Ftc-T cells (Figures 5F and 5G).

IFI27can promote cardiac fibroblast proliferation and collagen expression

Among the upregulated genes, we identified interferon alpha inducible protein 27 (*IFI27*), which was significantly enriched in CBMCs (Figure 6A-a), T cells (Figure 6A-b) and cluster 2 of T cells (Figure 6A-c) in the CSC of patients with PerAF. The t-SNE output illustrating cells expressing *IFI27* is presented in Figure S4. Flow cytometry and qRT-PCR further confirmed the upregulation of *IFI27*(Figures 6B and 6C), with a 3.27-fold increase in mean fluorescence intensity (MFI) ($p < 0.001$) (Figure 6D) in Ftc-T cells in the PerAF group compared to the PSVT group. This consistency between the scRNA-seq and the validation data reinforces the robustness of our findings.

To delve deeper into the role of IFI27 in promoting fibrosis, we explored its effects on the proliferation and collagen expression of CFs. *IFI27* over-expression, in contrast to control cells, resulted in an elevation in the expression of COL-1 and α-SMA (Figure 6E) and promoted CFs proliferation (Figure 6F). Conversely, *IFI27* knockdown yielded opposite effects (Figures 6E and 6F). These results suggested that IFI27 exerts a profibrotic effect.

Ftc-T cells and recurrence of PerAF post-CA

All PerAF patients from the validation cohort and the prospectively enrolled cohort completed a follow-up period of at least 6 months, with a median follow-up of 8 [7.0, 10.0] months. Among them, 22 patients experienced AF recurrence. Patient characteristics are summarized in Table 2. The FTR and FCR were significantly higher in the recurrence group than in the sinus rhythm (SR) group (Figures 7A and 7B). Univariate analysis suggested that FTR and FCR were independent risk factors for AF recurrence. Other risk factors included the duration of AF and left atrial diameter (LAD) (Table S8). After controlling for potential confounders such as LAD and duration (Model 1), Cox regression suggested that the crude recurrence rates were progressively higher with increasing FTR and FCR. Moreover, hazard ratios (HRs) maintained a similar trend in models 2 and 3 (Table 3). Therefore, FTR and FCR might be significantly and positively associated with AF recurrence. Additionally, we found that both the dose-response trajectories of FTR and FCR were linear (P linear = 0.0261 and 0.0251, P nonlinear = 0.4368 and 0.4753). Trajectories for FTR and FCR of model 1 were therefore plotted using the linear form and are shown in Figures 7C and 7E (FTR), Figures 7D and 7F (FCR). The recurrence risk HR (95% CI) associated with FTR was 1.34 (1.08–1.65), and for FCR, it was 1.39 (1.19–1.63) after adjustment for LA and duration of AF, suggesting that the trajectory was steeper for FCR than FTR.

The time-dependent ROC curve illustrated the predictive capacity of continuous values for FTR and FCR in AF recurrence, yielding AUROC values of 0.711 and 0.799, respectively. When comparing the AUROC of FTR with that of FCR, there was an increase of 0.088 for FCR, suggesting its potential superiority in discriminating patients at high risk of recurrence compared to FTR (Figure 7G). Optimal cut-off values for FTR and FCR, determined using the maximum Youden index, were 27.3% and 17.4%, respectively. These thresholds demonstrated sufficient sensitivity (0.875 and 0.938) and specificity (0.547 and 0.625) for predicting the risk of AF recurrence. Based on these cut-off values, individuals were categorized into the following groups: FTR-$_H$ (FTR$\geq$27.3%), FTR-$_L$ (FTR<27.3%), FCR-$_H$ (FCR$\geq$17.4%), and FCR-$_L$ (FCR<17.4%). Cox proportional hazard regression and survival analysis (Kaplan-Meier analysis) revealed that individuals with FTR-$_H$ and FCR-$_H$ had a significantly higher risk of recurrence, with hazard ratios (HRs) of 2.84 (1.03–7.86) and 10.42 (2.98–36.43) in Model 1 (Table 3; Figures 7H and 7I). Even after adjusting for other factors in Models 2 and 3, the risk of AF recurrence in the FTR-$_H$ and FCR-$_H$ groups remained significantly higher than that in the FTR-$_L$ and FCR-$_L$ groups.

A joint analysis of FTR and FCR with AF recurrence risk was further performed. The characteristics of patients in different groups are displayed in Table S9. Results from the joint analysis are shown in Table 4. In all models, AF recurrence risk was higher for patients with FTR-$_H$+FCR-$_H$ than for patients with only FTR-$_H$ or with only FCR-$_H$, which was indicative of an additional interaction. The survival curve also suggested that the AF recurrence in the FTR-$_H$+FCR-$_H$ group was significantly higher than that in the other groups, followed by the FTR-$_L$+FCR-$_H$ group (Figure 7J).

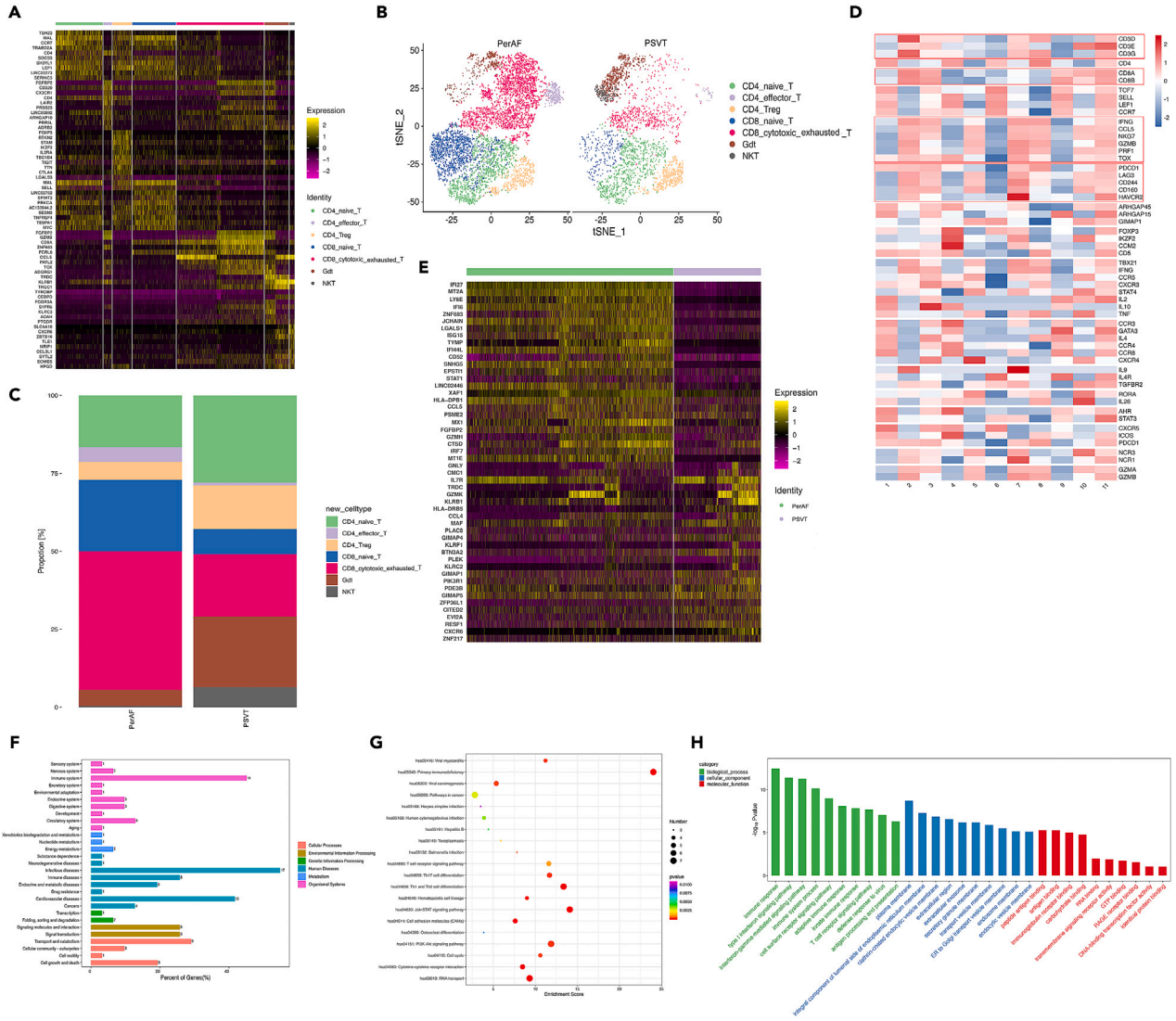

Figure 4. T cell subtypes from CBMCs between PerAF and PSVT subjects

(A) Heatmap of genes expressed by T cells from CBMCs between PerAF and PSVT subjects matching known marker genes of different T cell subsets.

(B) T-SNE projection plot of different T cells subtypes from CBMCs between PerAF and PSVT subjects.

(C) Abundance distribution of different T cell subtypes from CBMCs between the PerAF (left) and PSVT (right) subjects.

(D) Heatmap of marker genes of different T cell subsets matched with clusters of T cells from CBMCs between PerAF and PSVT subjects.

(E) Heatmap of top 25 DEGs of cluster #2 of T cells from CBMCs between PerAF and PSVT subjects.

(F) KEGG classification enrichment analysis of DEGs without immunoglobulin genes of cluster#2 of T cells from CBMCs between PerAF and PSVT subjects.

(G) KEGG pathway enrichment analysis of DEGs without immunoglobulin genes of cluster#2 of T cells from CBMCs between PerAF and PSVT subjects.

(H) GO enrichment analysis of DEGs without immunoglobulin genes of cluster#2 of T cells from CBMCs between PerAF and PSVT subjects. PerAF, persistent atrial fibrillation; PSVT, paroxysmal supra-ventricular tachycardia; T-SNE, T-distributed stochastic neighbor embedding; CBMCs, coronary sinus blood mononuclear cells; DEGs, differentially expressed genes; GO, gene ontology; KEGG, Kyoto Encyclopedia of Genes and Genomes.

DISCUSSION

To the best of our knowledge, this study represents the inaugural exploration of immune cell signatures within the CSC of PerAF patients by scRNA-seq. The primary findings reveal profound transcriptional alterations in T cell profiles within the CSC of PerAF patients, unveiling a T cell subset termed Ftc-T cells, predominantly comprised cytotoxic $CD8^+$ T cells and T-ex cells. Notably, Ftc-T cells were identified as potent promoters of CFs proliferation. Additionally, the study identifies FTR and FCR as significantly associated with AF recurrence, displaying a positive linear dose-response relationship. The top DEGs between PerAF and PSVT patients in CBMCs, T cells, and Ftc-T cells exhibited similarities. KEGG and GO enrichment analysis implicated these DEGs in immune diseases, inflammatory diseases, signaling pathways, cell growth,

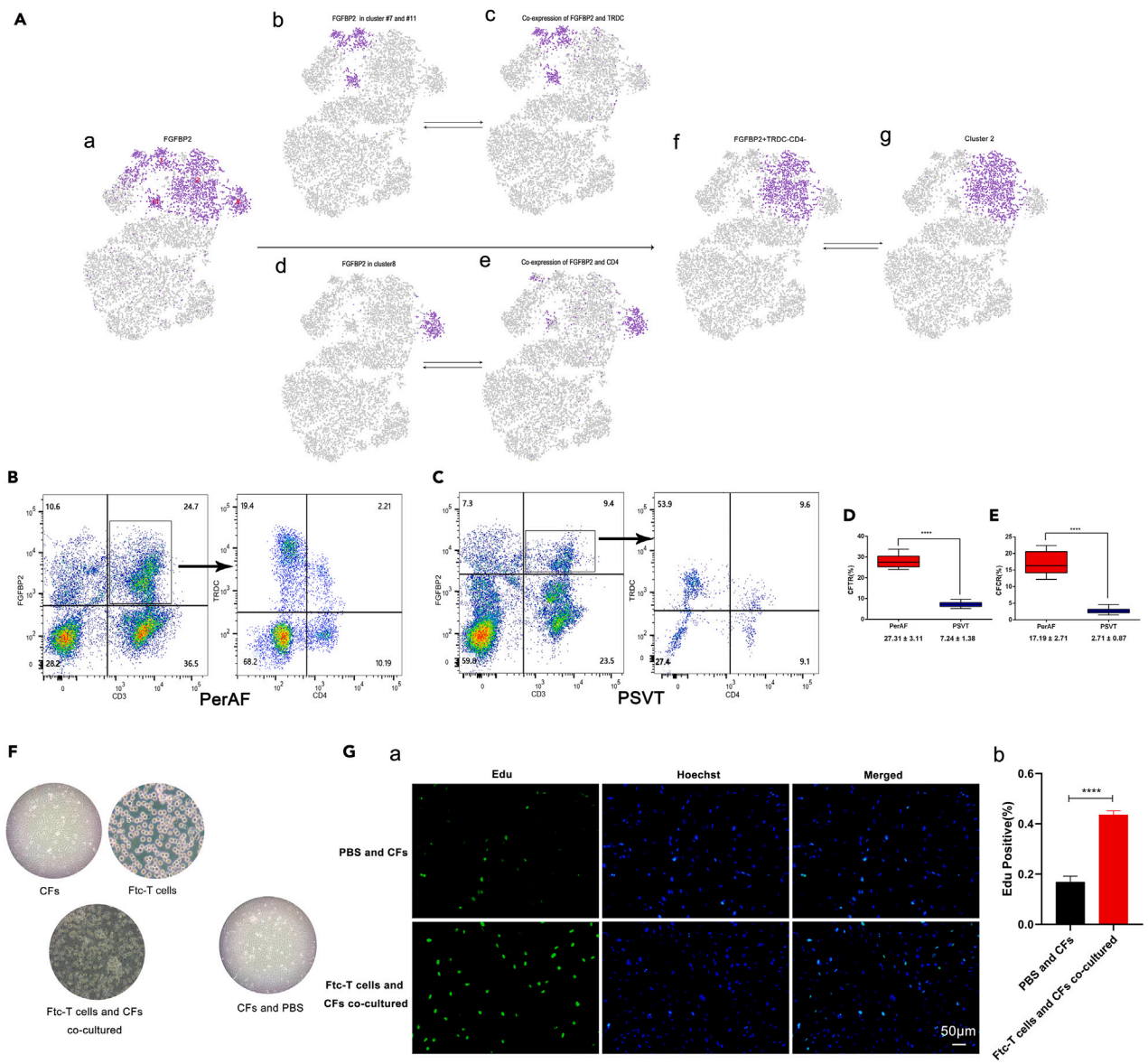

Figure 5. The redefinition and function of cluster#2

(A) T-SNE projection output of FGFBP2-expressing cells in T cells (a); T-SNE projection output of FGFBP2-expressing cells in cluster #7 and #11 of T cells from CBMCs (b); T-SNE projection output of cells co-expressing TRDC with FGFBP2 (c); T-SNE projection output of FGFBP2-expressing cells in cluster #8 of T cells from CBMCs (d); T-SNE projection output of cells co-expressing CD4 with FGFBP2 (e); T-SNE projection output of FGFBP2+TRDC-CD4$^-$cells (Ftc-T cells) of T cells from CBMCs (f); T-SNE projection output of cells of cluster #2 (g).

(B) Validation of the abundance of Ftc-T cells from CBMCs of the PerAF subjects by flow cytometry analysis in the validation cohort, N = 10 vs. 10.

(C) Validation of the abundance of Ftc-T cells from CBMCs of the PSVT subjects by flow cytometry analysis in the validation cohort, N = 10 vs. 10.

(D) Validation of FTR from CBMCs of PerAF (right) and PSVT (left) subjects by flow cytometry analysis in the validation cohort. N = 10 vs. 10, two-tailed unpaired Student's t tests, $p < 0.05$ indicating statistical significance, ****$p < 0.001$, ***∼**$p < 0.01$, *$p < 0.05$.

(E) Validation of FCR from CBMCs of PerAF (right) and PSVT (left) subjects by flow cytometry analysis in the validation cohort. N = 10 vs. 10, two-tailed unpaired Student's t tests, $p < 0.05$ indicating statistical significance, ****$p < 0.001$, ***∼**$p < 0.01$, *$p < 0.05$.

(F) Light microscopy view of Ftc-T cells co-cultured with CFs.

(G) Co-culture of Ftc-T cells with CFs can promote the proliferation of CFs. Representative images of EDU incorporation (green) reflecting cell proliferation (a) and quantification of EDU-positive cells (b). Data are means ± SEM (n = 3); ****$p < 0.001$, ***∼**$p < 0.01$, *$p < 0.05$. PerAF, persistent atrial fibrillation; PSVT, paroxysmal supra-ventricular tachycardia; T-SNE, T-distributed stochastic neighbor embedding; CBMCs, coronary sinus blood mononuclear cells; FTR, Ftc-T cells to the total T cells ratio; FCR, Ftc-T cells to the CBMCs ratio; CFs, cardiac fibroblasts.

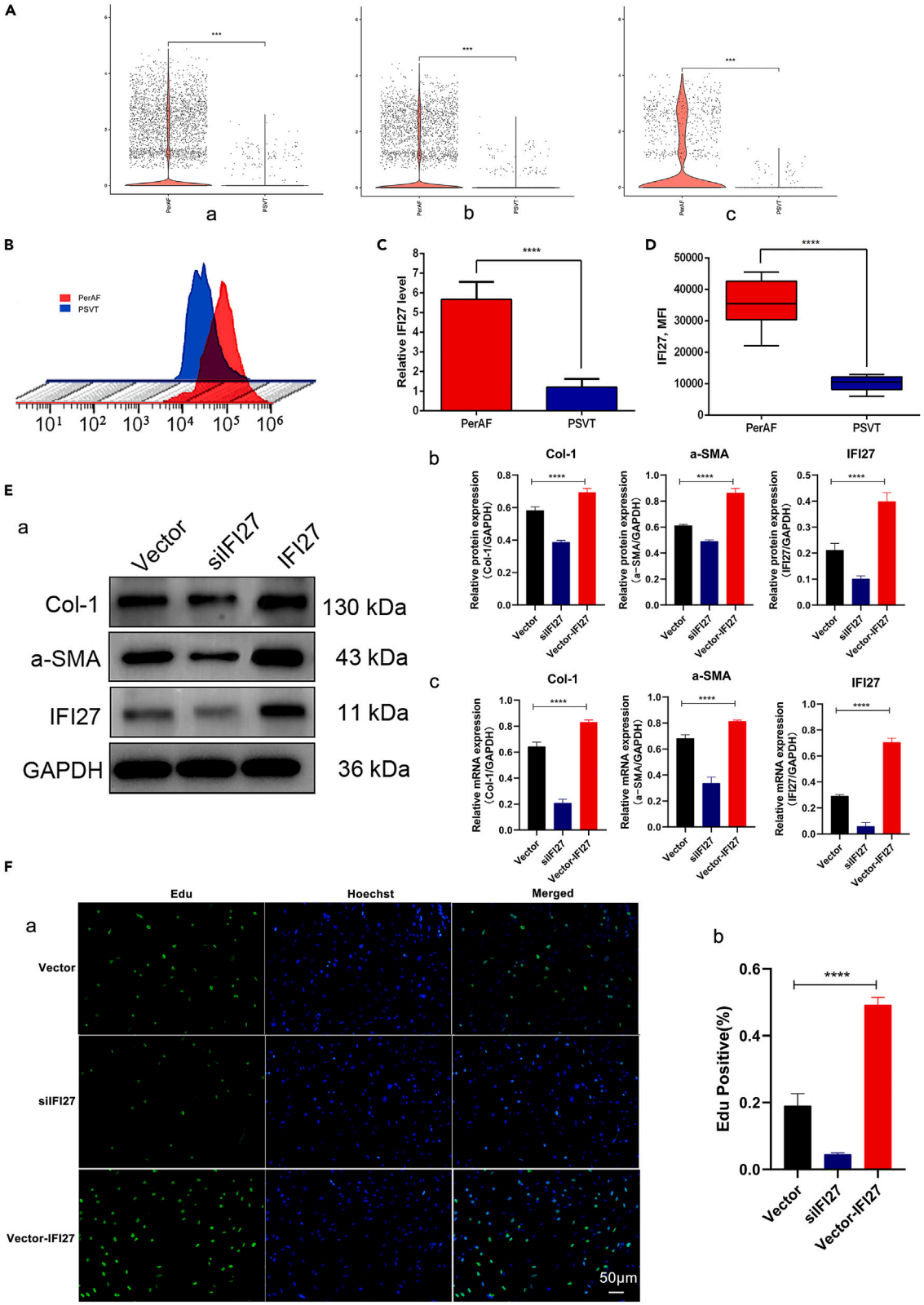
A
a
b
c
B
PerAF
PSVT
C
Relative IFI27 level
PerAF
PSVT
D
IFI27, MFI
PerAF
PSVT
E
a
Vector
siIFI27
IFI27
Col-1
a-SMA
IFI27
GAPDH
130 kDa
43 kDa
11 kDa
36 kDa
b
Col-1
a-SMA
IFI27
Relative protein expression (Col-1/GAPDH)
Relative protein expression (a-SMA/GAPDH)
Relative protein expression (IFI27/GAPDH)
Vector
siIFI27
Vector-IFI27
c
Col-1
a-SMA
IFI27
Relative mRNA expression (Col-1/GAPDH)
Relative mRNA expression (a-SMA/GAPDH)
Relative mRNA expression (IFI27/GAPDH)
F
a
Edu
Hoechst
Merged
Vector
siIFI27
Vector-IFI27
50μm
b
Edu Positive(%)
Vector
siIFI27
Vector-IFI27

Figure 6. Effect of *IFI27* on cardiac fibroblasts

(A) Differential expression of *IFI27* between PerAF and PSVT subjects. a: differential expression of *IFI27* in CBMCs between PerAF and PSVT subjects; b, differential expression of *IFI27* in T cells between PerAF and PSVT subjects; c, differential expression of *IFI27* in Ftc-T cells between PerAF and PSVT subjects. N = 10 vs. 10, Ftc-T cells: FGFBP2+TRDC-CD4$^-$ T cells, two-tailed unpaired Student's t tests, $p < 0.05$ indicating statistical significance, ****$p < 0.001$, ***∼**$p < 0.01$, *$p < 0.05$.

(B–D) Validation of the differential expression of *IFI27* in Ftc-T cells from CBMCs between PerAF and PSVT subjects. (B) Flow cytometry analysis of the differential expression of *IFI27* in Ftc-T cells from CBMCs between PerAF (red) and PSVT (blue) subjects; (C) High expression of *IFI27* in Ftc-T cells were identified in CBMCs of PerAF (right) than PSVT (left) subjects; (D) Validation of the differential expression of *IFI27* in Ftc-T cells from CBMCs between PerAF and PSVT subjects by qRT-PCR in the validation cohort. N = 10 vs. 10, Ftc-T cells: FGFBP2+TRDC-CD4$^-$ T cells, two-tailed unpaired Student's t tests, $p < 0.05$ indicating statistical significance, ****$p < 0.001$, ***∼**$p < 0.01$, *$p < 0.05$.

(E) Western blot (a, b) and qrt PCR (c) results showed that *IFI27* protein over-expression and knockdown can promote and inhibit the expression of col1 and a-SMA in CFs. Data are means ± SEM (n = 3); ****$p < 0.001$, ***∼**$p < 0.01$, *$p < 0.05$.

(F) *IFI27* protein overexpression and knockdown could promote and inhibit the proliferation of CFs. Representative images of EDU incorporation (green) reflecting cell proliferation (a) and quantification of EDU-positive cells (b). Data are means ± SEM (n = 3); ****$p < 0.001$, ***∼**$p < 0.01$, *$p < 0.05$.CFs: cardiac fibroblasts.

death, etc. Moreover, among the top DEGs in Ftc-T cells, *IFI27* was identified as capable of promoting CFs proliferation and collagen expression. Consequently, *IFI27*may be a potentially crucial factor in the progression of atrial fibrosis induced by Ftc-T cells, providing new insights into the underlying mechanisms through which Ftc-T cells may impact PerAF.

CA is an pivotal treatment for PerAF, however, its long-term efficacy is compromised, revealing individual heterogeneity likely arising from the continuous and personalized progression of atrial fibrosis.[16] The inflammatory response triggered by the ongoing infiltration of immune cells plays a pivotal role in the progression of atrial fibrosis.[12] CS, serving as the collection site for blood post-cardiac circulation, contains cardiac-specific information that may be richer than that found in peripheral blood.[14] Investigating the characteristics of immune cells in the CS may thus offer better insights into the impact of immune cells on inflammation and atrial fibrosis in PerAF.

A potential relationship between T cell immunity and the development of AF has been proposed.[17,18] Elevated CD4$^+$ T cells have been documented in the peripheral blood of AF patients. Moreover, circulating T helper 17 (Th17) cells have been linked to post-operative AF (POAF), with a higher Th17/Treg ratio positively correlated with AF risk.[19,20] While CD8$^+$ T cells have a pivotal cytotoxic role in immune diseases and viral infections, but little is known about their role in AF progression. Recently, CD8$^+$CD28^{null} T cells were proved to be an independent predictor for POAF.[21] In the present study, utilizing scRNA-seq, we unveiled substantial alterations in immune cells within the CS of PerAF patients, particularly a significant increase in T cells .Subsequent re-clustering of T cells led to the identification of a T cell subset termed Ftc-T cells, capable of promoting CF proliferation. Ftc-T cells were predominantly composed of CD8$^+$ T cells and T-ex cells, simplifying the potential involvement of CD8$^+$ T cells in PerAF progression. Furthermore, we reported for the first time that T-ex cells were significantly elevated in CSC of patients with PerAF. T-ex cells, representing CD8$^+$ T cells in a dysregulated state of "exhaustion" due to prolonged exposure to sustained immune stimulation, have been recognized for their immune significance in chronic viral infections and tumors.[22] The notable increase in T-ex cells in the CS of PerAF patients suggests their potential participation in the chronic and persistent inflammation associated with PerAF, even though the detailed mechanism remains unclear.

Followup data suggested that FTR and FCR were positively correlated with AF recurrence post-CA. On average, each additional 1% of FTR was associated with a 34% increase in multivariable-adjusted risk for AF recurrence. Dose-dependent increased risk of 39% was also observed

Table 2. Characteristics of patients after catheter ablation

	Overall (n = 80)	SR(n = 58)	Recurrence(n = 22)	p-value
Age, years	50 (45, 55)	50 (45, 55)	47 (44, 55)	0.63
Male, n (%)	52 (65.0%)	36 (62.1%)	16 (72.7%)	0.53
BMI, kg/m^2	22.8 ± 1.8	22.9 ± 1.6	22.5 ± 2.1	0.29
Duration of AF, months	8.0 (5.0, 11.0)	7.2 (5.2, 10.0)	11.0 (8.4, 13.2)	<0.01
e-GFR	99 (95,113)	102 (95,114)	98 (93,111)	0.45
Stroke	3	1	2	0.33
LVEF, %	58.8 (55.6, 60.9)	58.6 (55.6, 61.0)	59.1 (56.8, 60.5)	0.94
LAD, mm	42.0 ± 3.9	41.6 ± 3.9	43.0 ± 3.8	0.15
CHD, n (%)	23 (28.7%)	15 (25.9%)	8 (36.4%)	0.52
Hy, n (%)	39 (48.8%)	25 (43.1%)	14 (63.6%)	0.16
Follow-up, months	8.0 (7.0, 10.0)	8.0 (7.0, 10.0)	8.5 (7.3, 10.0)	0.36

Values are mean ± SD, median (interquartile range, IQR) or n (%). AF, atrial fibrillation, CHD, coronary heart disease, Hy, hypertension, BMI, Body mass index, LAD, left atrial diameter, LVEF, left ventricular ejection fraction. The statistical method used was Fisher exact test for comparison of categorical variables, and a Mann-Whitney U test for comparison of continuous variables. Statistical tests were 2-tailed, with $p < 0.05$ indicating statistical significance.

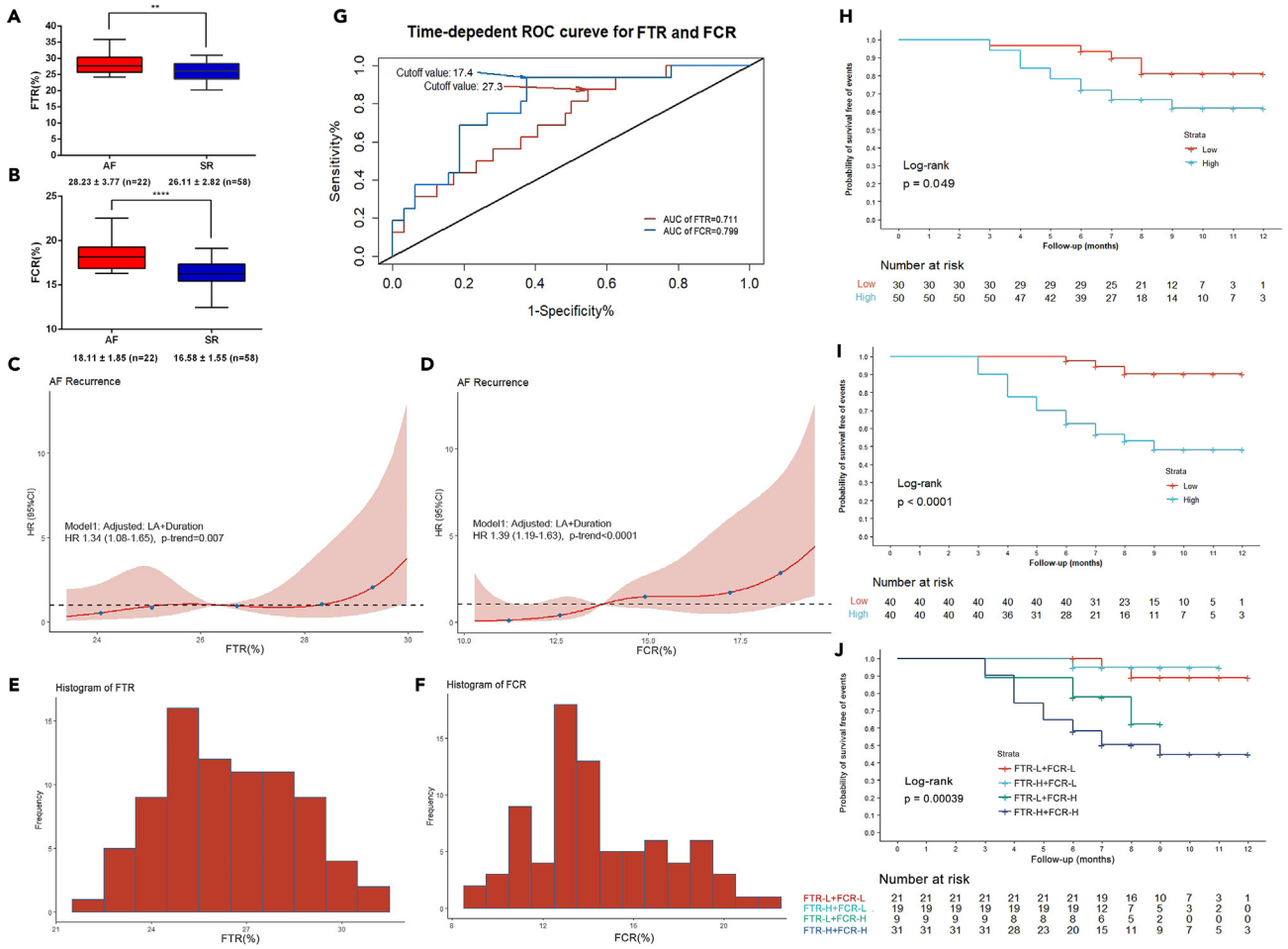

Figure 7. Ftc-T cells and recurrence of PerAF post-CA

(A) FTR in patients with AF recurrence (right, $n = 22$) and SR maintenance (left, $n = 78$) post-CA. Two-tailed unpaired Student's t tests, $p < 0.05$ indicating statistical significance, ****$p < 0.001$, ***∼**$p < 0.01$, *$p < 0.05$.

(B) FCR in patients with AF recurrence (right, $n = 22$) and SR maintenance (left, $n = 78$) post-CA. Two-tailed unpaired Student's t tests, $p < 0.05$ indicating statistical significance, ****$p < 0.001$, ***∼**$p < 0.01$, *$p < 0.05$.

(C and E) Continuous dose-response relationship between AF recurrence and FTR, estimated using linear Cox regression models.

(D and F) Continuous dose-response relationship between AF recurrence and FCR, estimated using linear Cox regression models.

(G) The time-dependent ROC curves for FTR and FCR for AF recurrence.

(H) Kaplan-Meier survival curves of patients free from AF for FTR-$_L$ and FTR-$_H$ group following ablation. Log rank test with $p < 0.05$ indicates statistical significance.

(I) Kaplan-Meier survival curves of patients free from AF for FCR-$_L$ and FCR-$_H$ group following ablation. Log rank test with $p < 0.05$ indicates statistical significance.

(J) Kaplan-Meier survival curves of patients free from AF for FTR-$_L$+FCR-$_L$, FTR-$_H$+FCR-$_L$, FTR-$_L$+FCR-$_H$ and FTR-$_H$+FCR-$_H$ group following ablation. Log rank test with $p < 0.05$ indicates statistical significance. PerAF, persistent atrial fibrillation; Ftc-T, FGFBP2+TRDC-CD4$^-$ T cells; CA, catheter ablation; FTR, Ftc-T cells to the total T cells ratio; FCR, Ftc-T cells to the CBMCs ratio; SR, sinus rhythm; ROC, receiver operating characteristic; FTR-$_L$, FTR<27.3%; FTR-$_H$, FTR>27.3%, FCR-$_L$: FCR<17.4%, FCR-$_H$: FCR>17.4%.

for each 1% increase in FCR. When FTR and FCR were jointly classified, PerAF patients with the FTR-$_H$ and FCR-$_H$ had the greatest AF recurrence risk. Even after adjusting for different confounding factors, the results also indicated that FTR and FCR could effectively predict recurrence post-CA. Therefore, Ftc-T cells may be the important immune cell subset that promotes the progression of PerAF.

ScRNA-seq analysis of DEGs of CBMCs, T cells, and Ftc-T cells subset from CSCs of PerAF patients showed significantly elevated *IFI27* expression. Emerging data suggest that *IFI27* is a mitochondrial protein, which can activate the Jak/STAT signaling pathway,[23] which not only can promote release of pro-inflammatory and pro-fibrotic factors and then facilitates the differentiation of fibroblasts into myofibroblasts,[24] but can also interact with AKT and MAPK/ERK pathways to promote tumor cells proliferation, growth, and migration.[25] In addition, *IFI27* was also found to be elevated in liver fibrosis and idiopathic pulmonary fibrosis tissues, suggesting that *IFI27* is closely related to tissue fibrosis.[26,27] Our study confirmed a substantial presence of Ftc-T cells highly expressing *IFI27* in the CSC of PerAF patients. Moreover, overexpression of *IFI27* significantly promoted the proliferation and collagen expression of CFs, while silencing *IFI27* inhibits CFs proliferation and

Table 3. Associations of AF recurrence with FTR and FCR

Models	FTR	*p*-value	FCR	*p*-value	$FTR\text{-}_H$ vs. $FTR\text{-}_L$	*p*-value	$FCR\text{-}_H$ vs. $FCR\text{-}_L$	*p*-value
Model 1	1.34 (1.08–1.65)	0.007	1.39 (1.19–1.63)	<0.0001	2.84 (1.03–7.86)	0.04	10.42 (2.98–36.43)	<0.0001
Model 2	1.33 (1.07–1.65)	0.011	1.31 (1.13–1.52)	<0.0001	2.72 (0.99–7.50)	0.052	8.45 (2.49–28.64)	<0.0001
Model 3	1.30 (1.05–1.62)	0.018	1.28 (1.11–1.49)	<0.0001	2.47 (0.90–6.78)	0.0785	8.19 (2.40–27.89)	<0.0001

Continuous variables (per 0.01). Model 1 = LA + Duration adjusted; Model 2 = age+sex adjusted; Model 3 = sex+BMI adjusted; LA, left atrial diameter, Duration, duration of AF; BMI, body mass index; AF, atrial fibrillation; HR, hazard ratio; CI, confidential interval; FTR, Ftc-T cell to total T cells ratio; FCR, Ftc-T cell to CBMCs ratio. FTR-L, Ftc-T cell to total T cells ratio<27.3%; FTR-H, Ftc -T cells to total T cells ratio>27.3; FCR-L, Ftc-T cells to CBMCs ratio<17.4%; FCR-H, Ftc-T cells to CBMCs ratio>17.4%. Data are expressed as HR (95% CI). Statistical tests were 2-tailed, with $p < 0.05$ indicating statistical significance.

collagen expression. Ftc-T cells continuously infiltrates the atrial tissue with the blood circulation, resulting in the enrichment of *IFI27* in the atrial tissue. This enrichment promotes fibroblasts transformation and proliferation through the release of pro-fibrotic factors, ultimately leading to the progression of atrial fibrosis. In addition, KEGG enrichment analysis of DGEs suggested the involvement of multiple genes in the JAK/STAT signaling pathway. Therefore,the JAK/STAT signaling pathway may have an important role in the promotion of atrial fibrosis by Ftc-T cells and *IFI27*. Ftc-T cells may participate in the pathological process of atrial fibrosis progression in PerAF through *IFI27* and, simultaneously, serve as potential target for immunological interventions in patients with PerAF.

In summary, scRNA-seq revealed the immune cells atlas of CSC in patients with PerAF, highlighting a high proportion of T cells and Ftc-T cell subset in the CSC of patients with PerAF.Ftc-T cells, in addition to promoting the proliferation of CFs, but high FTR and FCR are closely related to the recurrence of AF post-CA of PerAF. Furthermore, *IFI27* emerged as a potentially crucial factor in the progression of AF and may serve as a potential target for AF intervention.

Limitations of the study

Despite its numerous strengths, this study should be interpreted in light of some limitations. First, scRNA-seq technology has inherent constraints, such as a limited ability to infer cell-cell interactions and capture spatial information, necessitating supplementation with other technologies. Second, while this study represents the largest scRNA-seq investigation of immune cells in CSC of patients with PerAF to our knowledge, the number of subjects studied is limited. We cannot exclude the possibility that comorbidities, differences in risk factors, or therapies might have influenced the observed changes in gene expression patterns. Thirdly, although we identified a high-abundance T cell subset (Ftc-T cells) in the CSC of patients with PerAF, subsequent follow-up data demonstrated that this cell subset is closely related to the prognosis of PerAF, and suggested that *IFI27* may be a functional substance. However, this study has not been further verified through vivo experiments. Finally, the mechanism by which Ftc-T cells interact with *IFI27* in target cells remains unclear and necessitates further study.

STAR★METHODS

Detailed methods are provided in the online version of this paper and include the following:

- KEY RESOURCES TABLE
- RESOURCE AVAILABILITY
  - Lead contact
  - Materials availability
  - Data and code availability
- EXPERIMENTAL MODEL AND STUDY PARTICIPANT DETAILS
- METHOD DETAILS
  - Participants and coronary sinus blood collection
  - The inclusion and exclusion criteria for patients

Table 4. Joint associations of AF recurrence with FTR and FCR

Models	$FTR\text{-}_L$+$FCR\text{-}_L$	$FTR\text{-}_H$+$FCT\text{-}_L$	*p*-value	$FTR\text{-}_L$+$FCR\text{-}_H$	*p*-value	$FTR\text{-}_H$+$FCR\text{-}_H$	*p*-value
Model 1	1 (ref)	0.84 (0.07–9.55)	0.890	7.25 (1.12–46.92)	0.038	10.32 (2.27–47.07)	0.003
Model 2	1 (ref)	0.67 (0.06–7.51)	0.749	4.40 (0.73–26.46)	0.105	8.27 (1.88–36.24)	0.005
Model 3	1 (ref)	0.61 (0.05–6.77)	0.686	3.98 (0.65–24.33)	0.135	7.69 (1.74–33.96)	0.007

Continuous variables (per 0.01). Model 1 = LA + Duration adjusted; Model 2 = age + sex adjusted; Model 3 = sex + BMI adjusted; LA, left atrial diameter, Duration, duration of AF; BMI, body mass index; AF, atrial fibrillation; HR, hazard ratio; CI, confidential interval; FTR, Ftc-T cell to total T cells ratio; FCR, Ftc-T cell to CBMCs ratio. FTR-L, Ftc-T cell to total T cells ratio<27.3%; FTR-H, Ftc -T cells to total T cells ratio>27.3; FCR-L, Ftc-T cells to CBMCs ratio<17.4%; FCR-H, Ftc-T cells to CBMCs ratio>17.4%. Data are expressed as HR (95% CI). Statistical tests were 2-tailed, with $p < 0.05$ indicating statistical significance.

- Coronary sinus blood sampling
- CBMCs collection of CSB before single-cell RNA-seq
- Single-cell RNA-seq library preparation
- Single cell RNA library construction and sequencing
- Single-cell RNA-seq data analyses
- Single-cell RNA-seq data analyses
- Functional and pathway enrichment analysis
- Protein–protein interaction network analysis
- Flow cytometry and cell sorting
- Cardiac fibroblasts
- Plasmid construction and transfection
- Western blot assay
- Quantitative RT-PCR
- Co-culture of FCs and Ftc-T cells
- Detection of cells proliferation
- Follow-up

- QUANTIFICATION AND STATISTICAL ANALYSIS
  - Statistical analyses

SUPPLEMENTAL INFORMATION

Supplemental information can be found online at https://doi.org/10.1016/j.isci.2024.110127.

ACKNOWLEDGMENTS

We would like to thank Oebiotech (Shanghai) for supporting the scRNA experiment and sequencing. We thank Zi-long Xiao for help with flow cytometry and cell sorting. We are also thankful for the support from the Shanghai Institute of Cardiovascular Diseases for data analysis. W.Q.Z. was supported by the Science and Technology Commission of Shanghai Municipality, (Grant No. 21S31906902), K..C was supported by the Natural Science Foundation of Xinjiang Uygur Autonomous Region (No.2021D01C024).

AUTHOR CONTRIBUTIONS

C.F.C., K.C., W.Q.Z. and J.-B.G. conceptualized this project and supervised the overall experiments; C.F.C., J.W., and Y.L.L. performed bioinformatics analysis; C.F.C., K.C., Y.P., Y.X., and Q.X.C. completed patients base data collation, coronary sinus blood collections and clinical following-up data post-ablation, C.F.C. and Z.L.X. performed flow cytometry. C.-F.C. drew the schematic illustration. C.F.C., Q.X.C., K.C., Y.Z.X., W.Q.Z. and J.B.G. wrote, reviewed, and edited the manuscript.

DECLARATION OF INTERESTS

The authors declare no competing interests.

Received: January 10, 2023
Revised: June 9, 2023
Accepted: May 24, 2024
Published: May 27, 2024

REFERENCES

1. January, C.T., Wann, L.S., Calkins, H., Chen, L.Y., Cigarroa, J.E., Cleveland, J.C., Jr., Ellinor, P.T., Ezekowitz, M.D., Field, M.E., Furie, K.L., et al. (2019). 2019 aha/acc/hrs focusedupdate of the 2014 aha/acc/hrs guideline for the management of patients with atrial fibrillation: A report of the american college of cardiology/american heart association task force on clinical practice guidelines and the heart rhythm society in collaboration with the society of thoracic surgeons. Circulation *140*, e125–e151.
2. Kuck, K.H., Merkely, B., Zahn, R., Arentz, T., Seidl, K., Schlüter, M., Tilz, R.R., Piorkowski, C., Gellér, L., Kleemann, T., and Hindricks, G. (2019). Catheter ablation versus best medical therapy in patients with persistent atrial fibrillation and congestive heart failure: The randomized amica trial. Circ. Arrhythm. Electrophysiol. *12*, e007731.
3. Park, J.W., Yu, H.T., Kim, T.H., Uhm, J.S., Joung, B., Lee, M.H., and Pak, H.N. (2020). Mechanisms of long-term recurrence 3 years after catheter ablation of atrial fibrillation. JACC. Clin. Electrophysiol. *6*, 999–1007.
4. Hu, Y.F., Chen, Y.J., Lin, Y.J., and Chen, S.A. (2015). Inflammation and the pathogenesis of atrial fibrillation. Nat. Rev. Cardiol. *12*, 230–243.
5. Adamo, L., Rocha-Resende, C., Prabhu, S.D., and Mann, D.L. (2020). Reappraising the role of inflammation in heart failure. Nat. Rev. Cardiol. *17*, 269–285.
6. Yao, C., Veleva, T., Scott, L., Jr., Cao, S., Li, L., Chen, G., Jeyabal, P., Pan, X., Alsina, K.M., Abu-Taha, I., Dr, et al. (2018). Enhanced cardiomyocyte nlrp3 inflammasome signaling promotes atrial fibrillation. Circulation *138*, 2227–2242.
7. Van Wagoner, D.R., and Chung, M.K. (2018). Inflammation, inflammasome activation, and atrial fibrillation. Circulation *138*, 2243–2246.
8. Friedrichs, K., Klinke, A., and Baldus, S. (2011). Inflammatory pathways underlying atrial fibrillation. Trends Mol. Med. *17*, 556–563.
9. Zhang, Y., Qi, Y., Li, J.J., He, W.J., Gao, X.H., Zhang, Y., Sun, X., Tong, J., Zhang, J., Deng,

X.L., et al. (2021). Stretch-induced sarcoplasmic reticulum calcium leak is causatively associated with atrial fibrillation in pressure-overloaded hearts. Cardiovasc. Res. *117*, 1091–1102.
10. Adamsson Eryd, S., Smith, J.G., Melander, O., Hedblad, B., and Engström, G. (2011). Inflammation-sensitive proteins and risk of atrial fibrillation: A population-based cohort study. Eur. J. Epidemiol. *26*, 449–455.
11. Saigusa, R., Winkels, H., and Ley, K. (2020). T cell subsets and functions in atherosclerosis. Nat. Rev. Cardiol. *17*, 387–401.
12. Liu, Y., Shi, Q., Ma, Y., and Liu, Q. (2018). The role of immune cells in atrial fibrillation. J. Mol. Cell. Cardiol. *123*, 198–208.
13. Turer, A.T., Addo, T.A., Martin, J.L., Sabatine, M.S., Lewis, G.D., Gerszten, R.E., Keeley, E.C., Cigarroa, J.E., Lange, R.A., Hillis, L.D., and de Lemos, J.A. (2011). Myocardial ischemia induced by rapid atrial pacing causes troponin t release detectable by a highly sensitive assay: Insights from a coronary sinus sampling study. J. Am. Coll. Cardiol. *57*, 2398–2405.
14. Jaumdally, R., Varma, C., Macfadyen, R.J., and Lip, G.Y.H. (2007). Coronary sinus blood sampling: An insight into local cardiac pathophysiology and treatment? Eur. Heart J. *28*, 929–940.
15. Mabbott, N.A., Baillie, J.K., Brown, H., Freeman, T.C., and Hume, D.A. (2013). An expression atlas of human primary cells: Inference of gene function from coexpression networks. BMC Genom. *14*, 632.
16. Marrouche, N.F., Wilber, D., Hindricks, G., Jais, P., Akoum, N., Marchlinski, F., Kholmovski, E., Burgon, N., Hu, N., Mont, L., et al. (2014). Association of atrial tissue fibrosis identified by delayed enhancement mri and atrial fibrillation catheter ablation: The decaaf study. JAMA *311*, 498–506.
17. Hammer, A., Niessner, A., and Sulzgruber, P. (2021). The impact of $CD4^{+}CD28^{null}$ T lymphocytes on atrial fibrillation: a potential pathophysiological pathway. Inflamm. Res. *70*, 1011–1014.
18. Stone, E., Taylor, J., Kiat, H., and McLachlan, C.S. (2021). Machine learning based deconvolution of microarray atrial samples from atrial fibrillation patients reveals increased fractions of follicular cd4+ t lymphocytes and gamma-delta t cells. J. Physiol. Pharmacol. *72*, 957–963.
19. He, Y., Chen, X., Guo, X., Yin, H., Ma, N., Tang, M., Liu, H., and Mei, J. (2018). Th17/treg ratio in serum predicts onset of postoperative atrial fibrillation after off-pump coronary artery bypass graft surgery. Heart Lung Circ. *27*, 1467–1475.
20. Wang, X., Fan, H., Wang, Y., Yin, X., Liu, G., Gao, C., Li, X., and Liang, B. (2021). Elevated peripheral t helper cells are associated with atrial fibrillation in patients with rheumatoid arthritis. Front. Immunol. *12*, 744254.
21. Kazem, N., Sulzgruber, P., Thaler, B., Baumgartner, J., Koller, L., Laufer, G., Steinlechner, B., Hohensinner, P., Wojta, J., and Niessner, A. (2020). Cd8+cd28null t lymphocytes are associated with the development of atrial fibrillation after elective cardiac surgery. Thromb. Haemost. *120*, 1182–1187.
22. McLane, L.M., Abdel-Hakeem, M.S., and Wherry, E.J. (2019). Cd8 t cell exhaustion during chronic viral infection and cancer. Annu. Rev. Immunol. *37*, 457–495.
23. Xu, L., Zu, T., Li, T., Li, M., Mi, J., Bai, F., Liu, G., Wen, J., Li, H., Brakebusch, C., et al. (2021). Atf3 downmodulates its new targets ifi6 and ifi27 to suppress the growth and migration of tongue squamous cell carcinoma cells. PLoS Genet. *17*, e1009283.
24. Zhang, Q., Wang, L., Wang, S., Cheng, H., Xu, L., Pei, G., Wang, Y., Fu, C., Jiang, Y., He, C., and Wei, Q. (2022). Signaling pathways and targeted therapy for myocardial infarction. Signal Transduct. Target. Ther. *7*, 78.
25. Owen, K.L., Brockwell, N.K., and Parker, B.S. (2019). JAK-STAT Signaling: A Double-Edged Sword of Immune Regulation and Cancer Progression. Cancers *11*, 2002.
26. Domagalski, K., Pawłowska, M., Kozielewicz, D., Dybowska, D., Tretyn, A., and Halota, W. (2015). The impact of il28b genotype and liver fibrosis on the hepatic expression of ip10, ifi27, isg15, and mx1 and their association with treatment outcomes in patients with chronic hepatitis c. PLoS One *10*, e0130899.
27. Rostami, M.R., and Bradic, M. (2021). The derepression of transposable elements in lung cells is associated with the inflammatory response and gene activation in idiopathic pulmonary fibrosis. Mob. DNA *12*, 14.

STAR★METHODS

KEY RESOURCES TABLE

REAGENT or RESOURCE	SOURCE	IDENTIFIER
Antibodies		
Rabbit monoclonal anti-IFI27	Abcam	ab171919
Rabbit monoclonal anti-a-SMA	Abcam	ab244177
Rabbit monoclonal anti-Col-1	Abcam	ab270946
Rabbit monoclonal anti-GAPDH	Abcam	ab9485
Horseradish peroxidase (HRP) -conjugated secondary antibody	Abcam	ab205718
Biological samples		
Coronary sinus blood in patients with persistent atrial fibrillation	Zhongshan Hospital, Fudan university	N/A
Coronary sinus blood in patients with paroxysmal supraventricular tachycardia	Zhongshan Hospital, Fudan university	N/A
Chemicals, peptides, and recombinant proteins		
10% male human AB serum	Sigma-Aldrich	H4522
IL-2	Sigma-Aldrich	I4161
5′- ethynyl-2′-deoxyuridine	Sigma-Aldrich	BCK-EDU488
High-Capacity cDNA Reverse Transcription Kit	Thermo Fisher	15596–018
Nuclear and Cytoplasmic Protein Extraction Kit	Beyotime Biotechnology	NDC-RBB-XFA61F-1
BCA Protein Quantitative Detection Kit	Sigma-Aldrich	BCA1
PVDF membranes	Millipore	03010040001
Endo-Free Plasmid Maxi Kit	Omega	D6926
Lipofectamine 3000 reagent	Lipofectamine	L3000-008
Critical commercial assays		
GEXSCOPETM Single-Cell RNA Library Kit	Singleron Biotechnologies	N/A
Chromium Next GEM Single Cell 3′ Kit v3.1	10X Genomics	PN-1000269
Deposited data		
Single-cell RNA-seq raw and analyzed data	This paper; Sequence Read Archive (SRA) for Human (SRA-Human)	PRJNA1108417
Experimental models: Cell lines		
Primary rat cardiac fibroblasts	Procell	N/A
Oligonucleotides		
siRNA targeting sequence: siIFI27-1:CTGCAGAGAAGAGAACCAT	This paper	N/A
siRNA targeting sequence: siIFI27-2:TCTGGCTCTGCCGTAGTTT	This paper	N/A
GAPDH Primer, Forward: GCACGACTTCTTCAAGTCCGCCATGCC	This paper	N/A
GAPDHPrimer Reverse: AATCCGTTGACTCCGACCTTC	This paper	N/A
Col-1 Primer, Forward: TCTAGACATGTTCAGCTTTGTGGAC	This paper	N/A
Col-1 Primer Reverse: TCTGTACGCAGGTGGATTGGTG	This paper	N/A
a-SMA Primer, Forward: GTCCCAGACATCAGGGAGTAA	This paper	N/A
a-SMAPrimer Reverse: TCGGATAGCGTCAGGA	This paper	N/A
IFI27 Primer, Forward: TGCTCTCACCTCATCAGCAGT	This paper	N/A
IFI27Primer Reverse: CACAACTCCTCCAATCACAACT	This paper	N/A

(*Continued on next page*)

Continued

REAGENT or RESOURCE	SOURCE	IDENTIFIER
Recombinant DNA		
pLenti-CMV-MCS- SBP-3Flag-tRFP-F2A-Neo	GenePharma	N/A
pLKO.1-TRCcopGFP-2A-PURO	GenePharma	N/A
Software and algorithms		
ImageJ version 10 1.5i	Open source	https://imagej.nih.gov/ij/
FlowJo version 10	Open source	https://www.flowjo.com/
Metascape	Open source	http://metascape.org/gp/index.html
R version 4.0.2	Open source	https://www.r-project.org/
10x Genomics Cell Ranger	Open source	https://www.10xgenomics.com/

RESOURCE AVAILABILITY

Lead contact

Further information and requests for resources should be directed to and will be fulfilled by the Lead Contact, wenqing zhu (20111210013@fudan.edu.cn).

Materials availability

This study did not generate new materials.

Data and code availability

- Single-cell RNA-seq data have been deposited at SRA and are publicly available as of the date of publication. Accession numbers are listed in the key resources table. This paper analyzes existing, publicly available data. These accession numbers for the datasets (PRJNA1108417) are listed in the key resources table.
- All original code has been deposited at Code Ocean and is publicly available as of the date of publication. The capsule number is listed in the key resources table.
- Any additional information required to reanalyze the data reported in this paper is available from the lead contact upon request.

EXPERIMENTAL MODEL AND STUDY PARTICIPANT DETAILS

Human PATICIPANTS: a total 6 subjects for scRNA-seq were divided over two cohorts (PerAF-1,PerAF-2, PerAF-3; PSVT-1, PSVT-2,PSVT-3) to isolate immune cells from coronary sinus blood (CSB) for scRNA-seq, detailed patient information could be found in Table S10. Subsequently, 10 patients were enrolled in each cohort, and flow cytometric analysis was used to validate the subtype cells, detailed patient information could be found in Table S11. Next, we prospectively enrolled 80 patients with PerAF who underwent CA for subsequent follow-up. CSB samples of all participants were available for further flow cytometry analysis, detailed patient information could be found in Table S12. Informed consents were obtained from all subjects and the experiments with human subjects were approved by the Ethics Committees of Zhongshan Hospital.

CELL LINES: primary rat cardiac fibroblasts were cultured in DMEM-F12 at temperature: 37°C with 5% CO2.

METHOD DETAILS

Participants and coronary sinus blood collection

A total of 6 subjects for scRNA-seq were divided over two cohorts for a total of 6 participants (PerAF: $n = 3$, PSVT: $n = 3$) to isolate immune cells from coronary sinus blood (CSB) for scRNA-seq. Subsequently, 10 patients were enrolled in each cohort, and flow cytometric analysis was used to validate the subtype cells identified by scRNA-seq. Next, we prospectively enrolled 80 patients with PerAF who underwent CA for subsequent follow-up. CSB samples of all participants were available for further flow cytometry analysis. All clinical investigations were conducted in accordance with the principles in the Declaration of Helsinki. The protocol of the study was approved by the Ethics Committees of Zhongshan Hospital. Prior to any study procedure, all participants provided written informed consent.

The inclusion and exclusion criteria for patients

The inclusion criteria were as follow: (a) patients with symptomatic persistent AF or PSVT who received radiofrequency ablation (RF) for the first time at the department of cardiology at the zhongshan hospital, Fudan University; (b) age: 40< age <60 years old; (c) All patients signed an informed consent form according to the standards of the Institution. The exclusion criteria were as follow: (a) patients complicated with

valvular heart disease, heart failure (HF), diabetes, chronic renal failure (CRF), tumor, hematological diseases, autoimmune disease, etc; (b) transthoracic echocardiography of left atrial diameter (LAD) > 50 mm.

Coronary sinus blood sampling

Coronary sinus blood (CSB) sampling: participants were in supine position, the right femoral vein was punctured and a guide wire was inserted. Under the guidance of X-ray, the sheath was placed along the guide wire to the inferior vena cava ostium, and then the mapping electrode was inserted through the sheath to the distal end of the CS. The sheath is then inserted into the CS along the mapping electrode, and CS blood sample is finally drawn from the lateral hole of the sheath. The 6 mL of whole blood sample was collected in sodium citrate–containing cell preparation tubes (CPT Vacutainer; Becton Dickinson, Germany) for scRNA-Seq experiment.

CBMCs collection of CSB before single-cell RNA-seq

For cell populations that can be used for single-cell sequencing, we preprocess whole blood samples. 5 mL of blood was collected in sodium citrate–containing cell preparation tubes (CPT Vacutainer; Becton Dickinson, Germany). The samples were filtered through a 40 um cell sieve (Becton Dickinson, Germany) and transferred to a 15 mL centrifuge tube. These tubes, containing a Ficoll plug, were centrifuged at 1500 g for 20 min at 18°C, the supernatant was discarded, and 5-10 mL of erythrocyte lysate (Miltenyi, 130-094-183) was added to the pelleted cells. Let stand for 10 min at room temperature, then centrifuge at 500 g for 10 min at 18°C, discard the supernatant and repeat the above steps 1–2 times. The precipitated cells were resuspended and washed with 5 mL of DMEM medium, centrifuged at 300 g for 30 min at 18°C, the supernatant was discarded, and then resuspended with an appropriate amount of medium. The cell suspension concentration and cell viability were counted by a Luna cell counter.

Single-cell RNA-seq library preparation

In brief, the initial step consisted in performing an emulsion where individual cells were isolated into droplets together with gel beads coated with unique primers bearing 10x cell barcodes, UMI (unique molecular identifiers) and poly (dT) sequences. Reverse transcription reactions were engaged to generate barcoded full-length cDNA followed by the disruption of emulsions using the recovery agent and cDNA clean up with DynaBeads MyOne Silane Beads (Thermo Fisher Scientific, Germany). Bulk cDNA was amplified using a Biometra Thermocycler T Professional Basic Gradient with 96-Well Sample Block (98°C for 3 min; cycled 14×: 98°C for 5 s, 67°C for 20 s, and 72°C for 1 min; 72°C for 1 min; held at 4°C). Amplified cDNA product was cleaned with the SPRI select Reagent Kit (Beckman Coulter, USA). Indexed sequencing libraries were constructed using the reagents from the Chromium Single Cell 30 v2 Reagent Kit, as follows: fragmentation, end repair and A-tailing; size selection with SPRIselect; adaptor ligation; post-ligation cleanup with SPRIselect; sample index PCR and cleanup with SPRI select beads. Library quantification and quality assessment were performed using Bioanalyzer Agilent 2100 using a High Sensitivity DNA chip (Agilent Genomics, USA). Indexed libraries were equimolarly pooled and sequenced on two Illumina HiSeq4000 using paired-end 26 × 98 bp as sequencing mode by GenomeScan (Leiden, Netherlands).

Single cell RNA library construction and sequencing

Single-cell suspensions with 13105 cells/mL in concentration in PBS (HyClone) were prepared. The P3 library was constructed according to Singleron GEXSCOPETM protocol by GEXSCOPETM Single-Cell RNA Library Kit (Singleron Biotechnologies). Libraries of other samples were constructed by Chromium Next GEM Single Cell 30 Kit v3.1 (10X Genomics). Individual libraries were diluted to 4 nM and pooled for sequencing. Pools were sequenced on Illumina HiSeq XTen with 150 bp paired-end reads to obtain a sequencing depth of approximately 6.5K reads/cell and a 70–80% saturation level.

Single-cell RNA-seq data analyses

Single-cell expression data were processed using the Cell Ranger software pipeline (version 3.1.0) provided by 10×Genomics to perform quality control (unique molecular identifier count/gene, UMI/gene; mitochondrial genes), sample de-multiplexing, barcode processing, and single-cell gene counting. After scRNA-seq and aggregating all sample data from Cell Ranger, 77946 cells were yielded from sequencing of 2,251,874,418 PE-reads for further analysis. Sequencing libraries showed valid barcodes of 96.5%, sequencing saturation of 85% per sample, with an average of 93.6% of mapping reads to the genome. Total genes per sample averaged 22,879, with 1,764 genes per cell and 6,036 mean UMI counts per cell. Sequencing reads were aligned to the human reference genome GRCh38 using the Cell Ranger suite with default parameters. Principal component analysis (PCA) was performed to reduce the dimensionality, and the principal components were used to generate clusters by the graph-based algorithm. Cells were visualized using a 2-dimensional t-distributed stochastic neighbor embedding (t-SNE) algorithm. Cell types were identified according to the expression of canonical marker genes for each cluster. Single-cell type was identified by Single R package with the reference transcriptomic datasets 'Human Primary Cell Atlas'. FindMarkers" function of Seurat (version 3.1.1) was used for differential gene expression analysis between PerAF and PSVT groups using the Wilcox test. Only those with adjusted p value < 0.05 and |log2foldchange| > 0.58 were identified as DEGs. A false discovery rate (FDR) correction was jointly applied for all genes in the dataset.

Single-cell RNA-seq data analyses

Quality control

We processed the unique molecular identifier (UMI) count matrix using the R package Seurat (version 3.1.1). To remove low quality cells and likely multiplet captures, which is a major concern in microdroplet-based experiments, we applied a criteria to filter out cells with UMI/gene numbers out of the limit of mean value +/− 2-fold of standard deviations assuming a Guassian distribution of each cells' UMI/gene numbers. Following visual inspection of the distribution of cells by the fraction of mitochondrial genes expressed, we further discarded low-quality cells where >10% of the counts belonged to mitochondrial genes. After applying these QC criteria, single cells were included in downstream analyses. Library size normalization was performed with Normalize Data function in Seurat[1] to obtain the normalized count. Specifically, the global-scaling normalization method "LogNormalize" normalized the gene expression measurements for each cell by the total expression, multiplied by a scaling factor (10,000 by default), and the results were logtransformed.

Dimensionality reduction and clustering

The most variable genes were selected using FindVariableGenes function (mean. function = ExpMean, dispersion.function = LogVMR) in Seurat. Principal component analysis (PCA) was performed to reduce the dimensionality with RunPCA function in Seurat. Graph-based clustering was performed to cluster cells according to their gene expression profile using the FindClusters function in Seurat. Cells were visualized using a 2-dimensional t-distributed stochastic neighbor embedding (t-SNE) algorithm with the RunTSNE function in Seurat.

Markers gene and cells type identification

We used the FindAllMarkers function (test.use = bimod) in Seurat to identify marker genes of each cluster. For a given cluster, FindAllMarkers identified positive markers compared with all other cells. Then, we used the R package SingleR, a novel computational method for unbiased cell type recognition of scRNA-seq, with the reference transcriptomic datasets 'Human Primary Cell Atlas' to infer the cell of origin of each of the single cells independently and identify cell types. Differentially expressed genes (DEGs) were identified using the FindMarkers Function (test.use = MAST) in Seurat. p value <0.05 and |log2foldchange| > 0.58 was set as the threshold for significantly differential expression.

Functional and pathway enrichment analysis

Gene ontology (GO) and the Kyoto Encyclopedia of Genes and Genomes (KEGG) pathway enrichment analysis of DEGs were performed by Metascape (http://metascape.org/gp/index.html) (version 3.5). Results were visualized with the ggplot2 R package (https://ggplot2.tidyverse.org/) (version 4.1.3). The significantly enriched GO terms and KEGG pathways met the criterion of corrected $p < 0.05$ (supplementary information, STAR methods).

Protein–protein interaction network analysis

DEGs were imported into Metascape. Protein-protein interaction network analysis (PPI) was performed using Metascape following the protocol.

Flow cytometry and cell sorting

Candidate cell subsets were preliminarily determined according to the results of single-cell sequencing. Then, corresponding antibodies were selected according to the specific proteins expressed by the cell subsets, and the blood samples of participants subsequently enrolled were collected for subsequent analysis by FACS analysis using a FACSAria II cell sorter (BD Biosciences). Data were analyzed with FlowJo software (Tree Star).

Cardiac fibroblasts

Primary rat cardiac fibroblasts (CFs) were obtained from Procell (Wuhan, China). Cells were cultured in DMEM-F12 supplemented with 10% fetal bovine serum (FBS). The cells were incubated at 37°C in a humidified atmosphere containing 5% CO_2.

Plasmid construction and transfection

Expression plasmids for *IFI27* (NM_001130080.3) were purchased from GenePharma (Suzhou, China). The *IFI27* sequence was cloned into pLenti-CMV-MCS- SBP-3Flag-tRFP-F2A-Neo and pcDNA3.1 (+)-HA vectors. The target sequences used for shRNA or siRNA gene-silencing plasmids were as follows: siIFI27-1, CTGCA GAGAAGAGAACCAT; siIFI27-2, TCTGGCTCTGCCGTAGTTT. The sequences were inserted into pLKO.1-TRCcopGFP-2A-PURO (GenePharma, Suzhou, China). The amplified vectors were transformed into competent Escherichia coli DH5α cells (TSINGKE, Beijing, China) and confirmed by sequencing. The vectors were isolated sequentially using an Endo-Free Plasmid Maxi Kit (Omega, Norcross, GA, USA). Transient transfection was performed using Lipofectamine 3000 reagent (Invitrogen, Carlsbad, CA, USA) according to the manufacturer's instructions.

For stable cells, 2×10^5 CFs were seeded on 6-well plates. When the cells had grown to 70–80% confluence, we replaced with fresh DMEM-F12 (Invitrogen, Carlsbad, CA, USA) medium without FBS and used the IFI27 or shIFI27 virus to infect the cells. After incubating for 72 h, the stable cells were obtained by puromycin screening.

Western blot assay

Cells were lysed in radio-immunoprecipitation assay (RIPA) buffer (Thermo Fisher, MA, USA) containing protease inhibitor phenylmethanesulfonyl fluoride (PMSF) (Thermo Fisher, MA, USA). Nuclear and cytoplasmic proteins were separated using a Nuclear and Cytoplasmic Protein Extraction Kit (Beyotime Biotechnology, Shanghai, China) according to the manufacturer's protocol. The protein concentration was quantitatively analyzed using a BCA Protein Quantitative Detection Kit (Sigma-Aldrich, Darmstadt, Germany). Protein samples were separated on SDS-PAGE gel and transferred to PVDF membranes (Millipore, Billerica, MA, USA). The PVDF membranes were blocked with 5% skimmed milk at room temperature for 1 h and incubated overnight with the primary antibody at 4°C. They were then incubated with secondary antibodies at room temperature for 1 h and PVDF membranes were detected using a Meilunbio Pico Chemiluminescent Substrate (Meilunbio, Dalian, China). The membranes were then observed using a ChemiDoc Touch Imaging System (Bio-Rad, Hercules, CA, USA). Primary antibodies were as follows: anti-IFI27 (1:1000; Abcam, Boston,USA), anti-a-SMA (1:1000; Abcam, Boston,USA), anti-Col-1 (1:1000; Abcam, Boston,USA), and anti-GAPDH (1:10,000; Abcam, Boston,USA). GAPDH was used as the loading control. Horseradish peroxidase (HRP)-conjugated secondary antibody (1:3000; Cell Signaling Technology) was incubated for 1 h at room temperature. Super Signal West Femto Substrate Trial Kit (Thermo Fisher, MA, USA) was used for chemiluminescence detection. The immunoreactive bands were analyzed in triplicate with ImageJ software (National Institutes of Health, Bethesda, MD, USA).

Quantitative RT-PCR

An TRIzol (Thermo Fisher, MA, USA) was used to extract total RNA following the manufacturer's protocol. Reverse transcription PCR and qRT-PCR were performed using High-Capacity cDNA Reverse Transcription Kit (Thermo Fisher, MA, USA) and SYBR Green Master Mix Kit (Thermo Fisher, MA, USA) using the ABI ViiA7 Real-Time PCR system (Thermo Lifetech, Carlsbad, CA, USA) under the following conditions: 95°C for 30 s and then 50 cycles of 95°C for 5 s and 60°C for 30 s.

Co-culture of FCs and Ftc-T cells

Culture media for Ftc-T cells were composed of RPMI 1640 (Gibco), supplemented with 2 mM Ultraglutamine I, 1:100 penicillin/streptomycin and 10% male human AB serum (Sigma-Aldrich) ("T cell medium"). One day before co-culture, Ftc-T cells were thawed in pre-warmed (37°C) T cell medium (human serum was replaced with FBS during thawing) and incubated for 15 min with 25 U/mL benzonase (Merck). After washing, cells were re-suspended at 2×10^6 cells/mL in T cell medium supplemented with 150 U/mL IL-2 and cultured overnight at 37°C. Prior to co-culture, CFs from earlier passages 3′ were seeded into a 6-well and cultured in DMEM-F12, supplemented with 10% FBS in cell culture incubator (37°C, CO2). When CFs grew to 60–70% confluence, we co-cultured them with Ftc-T cells.

Detection of cells proliferation

Cell proliferation was examined by 5′- ethynyl-2′-deoxyuridine (Edu, 10 μM). Cells were transferred into 96-well plates and cultured at 37°C overnight. Edu was incubated for 4 h before cells were fixed and permeabilized. Click-iT Edu Alexa Flour 488 imaging kit (Life Technologies, Eugene, OR, USA) was used according to the manufacturer's instructions. Images were captured at ten randomized fields by using light microscopy (Nikon Eclipse Ti-S; Nikon, Tokyo, Japan).

Follow-up

After discharge, the patients were scheduled for follow-up visits with baseline electrocardiogram (ECG), 24 h Holter monitoring and transthoracic echocardiography at 3, 6, 12, 18, and 24 months. Additional telephonic interviews were conducted regularly. In the case of symptoms suggestive of recurrent arrhythmia, additional visits were recommended. The first 3 months post ablation were designated as a 'blanking period'. A recurrence of arrhythmia during this time was not considered as an efficacy endpoint failure. After blanking period, recurrence of arrhythmia is defined as recurrence of AF or atrial tachycardia (≥30 s in duration on ECG monitoring). Until 8/2022, all patients were followed up for at least 6 months.

QUANTIFICATION AND STATISTICAL ANALYSIS

Statistical analyses

All analyses were conducted using R (version 4.1.3, R Foundation for Statistical Computing, Vienna, Austria) or SPSS (version 29.0, IBM, Armonk, NY, USA). Categorical variables were presented as frequency, and continuous variables were described as mean ± SD or median (interquartile range, IQR). Continuous variables were compared using Student's t test (normal distribution) or Mann–Whitney U (nonnormal distribution) tests. Proportions for categorical variables were compared using the Pearson chi-square test. The Fisher exact test was used when the data were limited. Statistical tests were 2-tailed, with $p < 0.05$ indicating statistical significance (****$p < 0.001$, ***∼**$p < 0.01$, *$p < 0.05$).

Hazard ratios (HRs) and 95% CIs for AF recurrence were estimated with Cox proportional hazards regression. Three Cox models were examined for outcome. Model 1 was adjusted for LA and duration of AF, model 2 was adjusted for potential confounders: age and sex, and Model 3 was adjusted for sex and BMI. Tests of linear trend were computed with Cox models that treated FTR and FCR as continuous variables. Proportional hazards assumptions were assessed with tests based on Schoenfeld residuals, and no variables violated the assumption.

The dose-response relation of AF recurrence with the continuous variables FTR and FCR were examined by means of 2 steps. First, we tested the dose-response trajectory for nonlinearity by repeating model 1 after including restricted cubic spline functions of FTR and FCR using the Regression Modeling Strategies (rms) package in R (R Foundation for Statistical Computing; Vienna, Austria). To test whether the shapes of the dose-response trajectories were sensitive to the number of knots used, we ran models with 3, 4, 5 knots, respectively, and R2 was used to assess power of model. Plots of the dose-response trajectories were reviewed for outcome for each model fit, and $\chi 2$ tests for nonlinearity were performed. After determining the most appropriate functional form of the dose-response trajectories, we plotted them for each outcome. Dose-response trajectories were plotted for model 1 to visualize the influence of adjustment. The model with 5 knots was identified with meaningfully different of trajectories and largest value of R2, so $\chi 2$ tests were performed for models with 5 knots to maximize statistical power.

The time-dependent receiver operating characteristic (ROC) curves were analyzed using the survival ROC package in the R platform to determine cut-off values with the largest Youden index for FTR and FCR. A C-statistic for the Cox model was applied to show the performance of FTR and FCR (area under of receiver-operating characteristic curve [AUROC]) in predicting the risk of AF recurrence in the cohort. The selection of the optimal FTR and FCR cut-off point was based on the highest Youden index. Results from all multivariable analyses are reported as HR with 95% CIs or coefficients. All statistical parameters are indicated in the figure legends or table footnote.

To explore the association of jointly classified FTR and FCR with AF recurrence, we categorized our sample into high and low FTR and high and low FCR by cut off value of time-depedent ROC, to create the following 4 mutually exclusive groups: low FTR, low FCR (reference group); low FTR, high FCR; high FTR, low FCR; and high FTR, high FCR. The HR for each jointly classified exposure group associated with AF recurrence was then estimated using the model 1. For Kaplan-Meier plot and patients at risk, a log rank test was used to compare the AF recurrence-free survival among different groups.